Sensitivity of torrential rain events to the sea surface temperature based on high-resolution numerical forecasts

Cindy Lebeaupin, Véronique Ducrocq, Hervé Giordani

Sensitivity of torrential rain events to the sea surface temperature based on high-resolution numerical forecasts

C. Lebeaupin,[1] V. Ducrocq,[1] and H. Giordani[1]

Received 29 July 2005; revised 1 February 2006; accepted 22 March 2006; published 30 June 2006.

[1] Torrential rains often occur in the western Mediterranean region during the fall season when the Mediterranean Sea is still warm. The Mediterranean Sea acts in moistening and warming the low level of the atmosphere. Then, the southerly to easterly flow that prevails before and during torrential rainfall events, transports the conditionally unstable air toward the coasts where the convection can develop often triggered by a flow interaction with orography. This study examines the sensitivity to the sea surface temperature (SST) of very short range (18–24 hours) high-resolution (2.4 km) forecasts of heavy precipitation events. Three torrential rainfall events were selected as representative of extreme rainfall events that occurred over southern France: two cases of quasi-stationary mesoscale convective systems and one other case characterized by a slow moving frontal perturbation. For each case, a number of runs is performed with the MESO-NH research model using several SST fields differing in their resolution or/and their average value over the Mediterranean basin. Results show that an increase (a decrease) of SST by several degrees, on average, intensifies (weakens) the convection. The convection can even be stopped with strong decrease of SST. Impacts on the stationary behavior of the systems have also been pointed out. A more detailed SST field influences the mesoscale patterns of the sea surface heat fluxes but have almost no significant effect on the convection and the low-level jets forecast. Eventually, the SST has been allowed to evolve during the runs through the action of the air-sea interface fluxes, resulting in local effects such as significant cooling of the SST beneath the low-level jet but almost no impact on the very short range forecasts of heavy precipitation.

Citation: Lebeaupin, C., V. Ducrocq, and H. Giordani (2006), Sensitivity of torrential rain events to the sea surface temperature based on high-resolution numerical forecasts, *J. Geophys. Res.*, *111*, D12110, doi:10.1029/2005JD006541.

1. Introduction

[2] The western Mediterranean region is prone to torrential rainfall during the fall season. These events characterized by large precipitation amount (typically more than 100–200 mm in less than 24 hours), can lead to severe flash floods, causing substantial damages and human casualties. Blocking synoptic situations, stationary in time and space, favor the occurrence of these torrential rainfall episodes [*Doswell et al.*, 1998; *Homar et al.*, 2002; *Ducrocq et al.*, 2003a]. Large amounts of precipitation can be accumulated during several-day periods when one or more frontal perturbations stay over the western Mediterranean area. The region's relieves (Alps, Massif Central and Pyrenees, see Figure 1) frequently slow the progression of the front and may enhance the rainfall intensity. However, in most cases, heavy precipitation are induced by Mesoscale Convective Systems (MCS) that remain over the area for several hours, leading to large rainfall amount in less than one day. Almost always, these MCSs are associated with a southerly to south-easterly low-level jet advecting moist air from the Mediterranean Sea. Therefore the Mediterranean Sea, still warm during the fall season, acts as a source of moisture and heat and contributes to increase the conditional convective instability.

[3] It is well recognized that the sea surface temperature (SST) plays a key role in tropical phenomena such as monsoons [*Gao et al.*, 2003; *Rowell*, 2003] or cyclones whose intensification strongly depends on the air-sea interface fluxes [*Shade and Emanuel*, 1999; *Bender and Ginis*, 2000; *Bao et al.*, 2000]. At midlatitudes, the mesoscale transfer of heat, moisture and momentum across the air-sea interface influences the dynamics and thermodynamics of the Marine Atmospheric Boundary Layer (MABL). When anticyclonic conditions prevail, oceanic fronts can alter the thermal and dynamical structures of the MABL and induce ageostrophic circulations by differential heating, as in breeze regimes [*Giordani et al.*, 1998; *Giordani and Planton*, 2000]. In cyclonic conditions, the intense fluxes associated with high SST, can destabilize the MABL and increase the cyclogenesis intensity during its initial stage [*Homar et al.*, 2003; *Giordani and Caniaux*, 2001]. *Weill et al.* [2003] showed by comparing modeled fluxes and observed fluxes in five measurements campaigns that using mesoscale SST data allows a better representation of heat fluxes, and

[1]Centre National de Recherches Meteorologiques, Météo-France, Toulouse, France.

0148-0227/06/2005JD006541

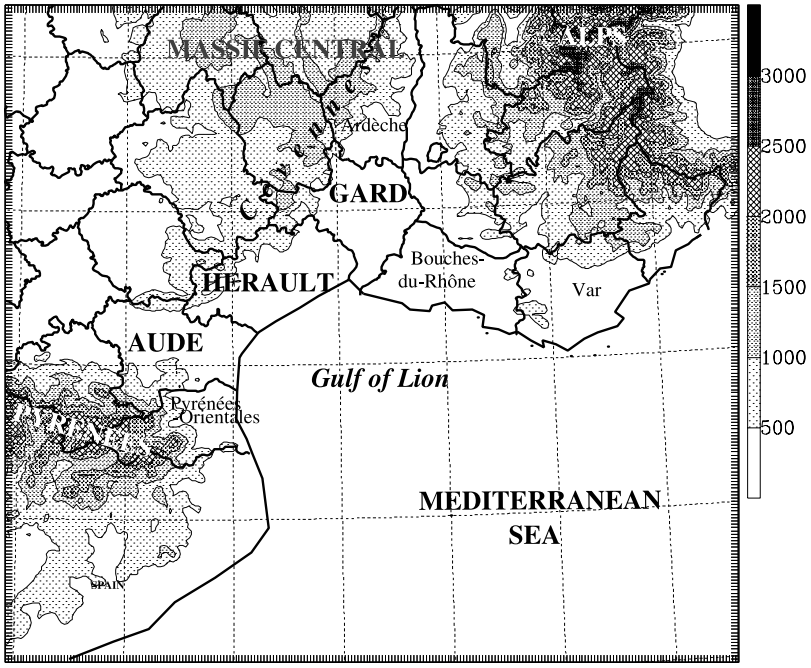

Figure 1. Southeastern France region: reliefs (grey scale in m) and departments (thick contours). A department is a subdivision of France administered by a prefect.

therefore a better simulation and understanding of the MABL dynamics.

[4] In the past, some studies have also paid attention to the role of the SST in western Mediterranean rainfall events. Several modeling studies have focused on the impact of SST on MCS development occurring over the Spanish coasts [*Millan et al.*, 1995; *Romero et al.*, 1997; *Pastor et al.*, 2001; *Homar et al.*, 2003]. From sensitivity experiments to the SST (warming or cooling between ±2°C and 5°C) or to the surface fluxes (by suppressing latent or sensible heat fluxes over the sea), *Millan et al.* [1995] showed that the higher the SST is, the more intense is the evaporation and stronger is the convection. The warming and moistening of the boundary layer due to the air-sea interface fluxes contributed to destabilize the air mass which is then transported by the low-level jet toward the mountains where conditional convective instability might be released. On the contrary, with colder SST or without evaporation from sea, the simulated rainfall totals are weaker, but without a complete vanishing of the convective developments. These effects increase with the forecast range, with in some cases no significant effect for the first 0–12 hour range as found by *Romero et al.* [1997]. Most of these sensitivity tests have been carried out using hydrostatic models with parameterized convection. Only *Pastor et al.* [2001] used a high-resolution nonhydrostatic model (RAMS) with a 2.5-km mesh allowing an explicit resolution of the convection. They examined the sensitivity to the SST for two cases of torrential rainfall in the area of Valence (Spain) by using different SST fields (monthly climatologies, real-time NOAA satellite). They showed a significant improvement of the precipitation forecast in term of both intensity and location, compared to the observations, when the SST field is based on the NOAA satellite product. They also argued that the maximum value of simulated precipitation is directly related to the value of the averaged SST over the basin.

[5] The purpose of our study is to examine the sensitivity of high-resolution simulations of Mediterranean intense rain events to the SST and to give some insights into the required details and quality needed for the SST field to be used by the next operational high-resolution short-range NWP systems. It may be viewed as an extension of *Pastor et al.'s* [2001] study on several aspects. First, we focus on representative torrential events that occurred over southeastern France. Second, besides using SST fields from different data sources, we also apply constant increase or decrease of the SST over the Mediterranean basin in order to estimate the response of the heavy precipitation systems to this extreme surface modification. Eventually, instead of forcing the model with the same SST field during all the simulations, the SST is introduced as a prognostic variable governed by the heat and radiation fluxes at the air-sea interface. This basic coupling aims at quantifying the impacts of an interactive rough oceanic mixed layer on the atmosphere. Three intense rain events have been selected and simulated with the French research mesoscale MESO-NH model [*Lafore et al.*, 1998]. The first two cases are two remarkable extreme flash-flood events that occurred over southeastern France (Aude case: 12–13 November 1999 and Gard case: 8–9 September 2002). For these two cases, long-lived quasi-stationary MCS induced huge amount of precipitation, with rainfall exceeding 500 mm in 24 hours. The third case (*Hérault* case: 3 December 2003) belongs to a different category of meteorological events that lead to flood over the region. From 1 to 3 December 2003, a slow moving frontal system with embedded convection stayed over the region. We concentrate here on the third day characterized by a more embedded convective activity. A reference simulation is first performed for each case using a real-time in situ SST

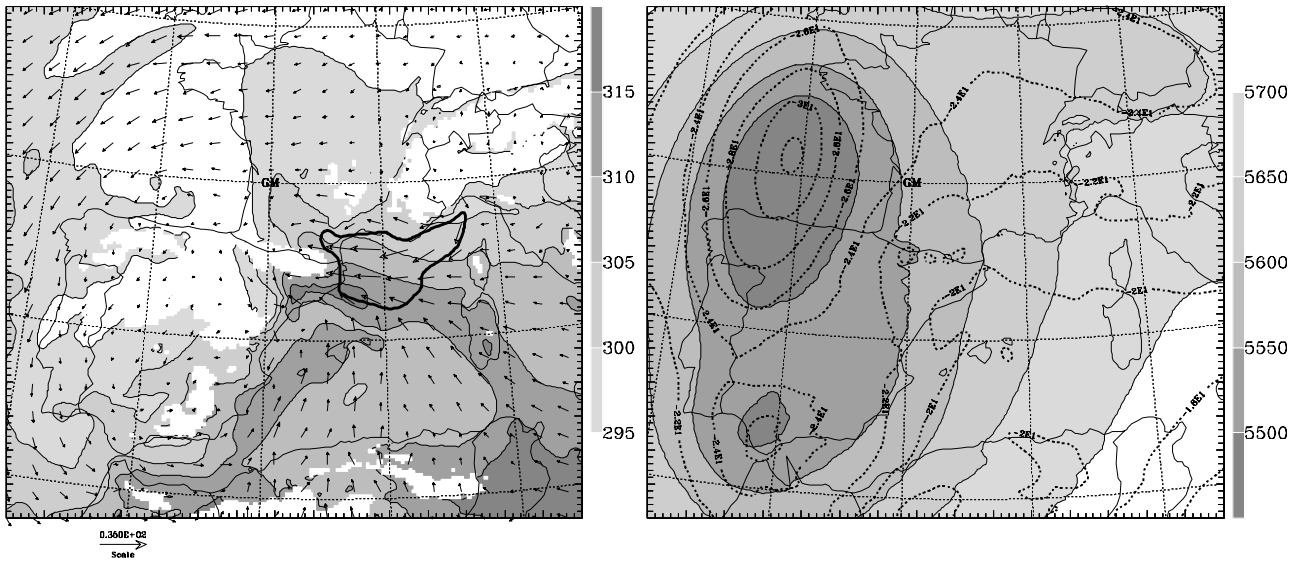

Figure 2. Aude case: ARPEGE analysis at 1200 UT, 12 November 1999. (left) Equivalent potential temperature (K) at 900 hPa in grey tones with thin contours and 35 m AGL wind vectors (m s^{-1}). The thick line delineates the areas with winds superior to 15 m s^{-1}. (right) Geopotential (m) at 500 hPa in grey tones and solid contours and temperature (°C) at 500 hPa in dotted lines.

analysis. As the model succeeds in simulating realistic intense rain events, this control runs serves as reference for the other numerical experiments. The sensitivity to the SST is then evaluated through departures from the reference experiment.

[6] The paper is organized as follows. The meteorological events are presented in section 2 and the characteristics of the simulations are described in section 3. Then, results of the simulations using different SST fields and using a prognostic SST are discussed in section 4, followed by a discussion and summary in section 5.

2. Overview of the Events

2.1. Aude Case: 12–13 November 1999

[7] The rainfall event and the meteorological environment in which the MCS develops are described in detail by *Bechtold and Bazile* [2001] and by *Ducrocq et al.* [2002, 2003a]. Only a short description of the event is provided here.

[8] On 12 November 1999 at 1200 UT (Figure 2), an upper level low-pressure area centered over Spain and southern France induced a vast southerly flow from North Africa to southern France. The upstream Palma sounding at 1200 UT, 12 November 1999 (not shown, see *Ducrocq et al.* [2002]) indicated high conditional instability (CAPE of the most unstable parcel about 1500 J kg^{-1}) associated with this southerly flow. Inside the warm air mass advected from the south, surface lows formed and accelerated the low-level easterly to south-easterly jet over the Mediterranean Sea. The winds reached more than 50 kts inside the moist low-level jet. The convergence is also enhanced by the deflection of the low-level flow by the southern Alps.

[9] The region was affected by light precipitation since 11 November. The intense convective rainfall started around 1500 UT, 12 November. Convection organized in a quasi-stationary mesoscale convective system that stayed over the Aude region from 1500 to 0000 UT. This MCS was characterized by a V shape in the infrared imagery [*Scofield*, 1985], whereas beneath the precipitation were organized in a narrow quasi-stationary line. Most of the high precipitation totals that have been recorded can be attributed to the MCS. In the town of Lézignan-Corbières (Aude department), the surface rainfall totals reached the maximum value of 624 mm in less than 48 hours, 551 mm of which fell in a 24-hour period. The area, which had received more than 200 mm in 48 hours, extended more than 150 km in length and about 50 km in width. During the night between 12 and 13 November, the upper level pressure low pivoted, pushing the southerly flow away over north Italy. At the same time convection moved eastward, and decayed. More than 30 people were killed as a result of this severe flash-flood event.

2.2. Gard Case: 8–9 September 2002

[10] This case is described from a meteorological and hydrological point of view by *Delrieu et al.* [2005] and *Ducrocq et al.* [2004]. Briefly, the synoptic situation was as follows.

[11] During the morning of 8 September 2002, an upper level cold pressure low was centered over Ireland and extending to the Iberian Peninsula, resulting in a southwesterly diffluent flow over southeastern France (Figure 3). Associated with the upper level low-pressure area, a surface cold front undulated over western France. An intense southerly low-level flow established over the Mediterranean coast. The atmosphere was conditionally unstable with CAPE reaching 850 J kg^{-1} on the midnight Nîmes radiosounding of 8 September (not shown, see *Ducrocq et al.* [2003b]).

[12] First convective cells developed over the Mediterranean Sea around 0400 UT, 8 September 2002, in the warm sector of the perturbation well ahead of the cold front. Then the convective cells progressed northward until reaching the

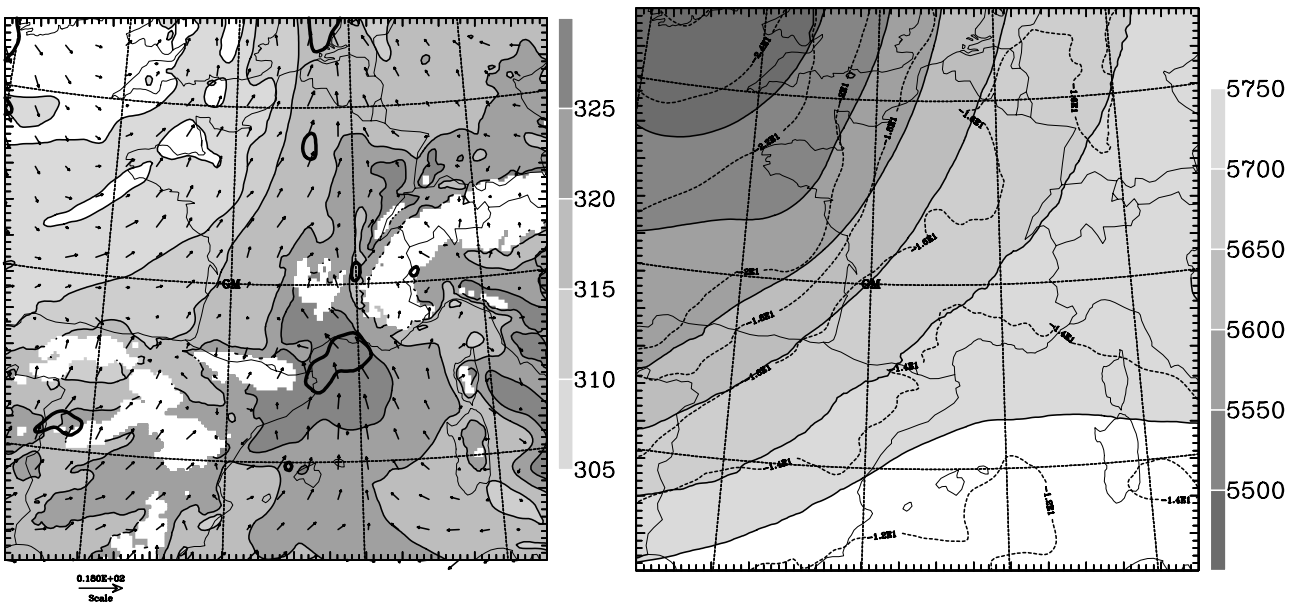

Figure 3. Gard case: As in Figure 2 but at 1200 UT, 8 September 2002. The thick lines on the left plot delimit areas with wind superior to 7 m s^{-1}.

continent around 0800 UT. Convection organized in a MCS and became quasi-stationary around 1200 UT. As for the Aude case, the cloud shield took on a V shape in the infrared imagery. Its convective part affected mainly the Gard region, whereas the stratiform precipitation extended northward. The MCS stayed over the region for almost 24 hours. During the afternoon of 8 September, the cold front progressed slowly to the east while the upper low pivoted to a NW/SE axis. During the night between 8 and 9 September, the cold front and the MCS collided, and the frontal system with its embedded convection moved away from the Gard region in the late morning of 9 September. Because of the stationary behavior of the MCS, surface rainfall totals reached paroxysmal values: 691 mm in 24 hours were recorded close to the city of Alès (Gard Department). This flooding resulted in more than 20 fatalities.

2.3. Hérault Case: 3 December 2003

[13] A heavy rainfall episode affected the French Mediterranean areas from 30 November 2003 to 4 December 2003. On 1 December, an upper level low-pressure area centered over Spain established a vast and intense southerly flow over southern France. A cold surface front undulated from northern to southeastern France. The frontal perturbation stayed over southeastern France until 3 December, resulting in 3-day accumulated precipitation reaching about 300 mm over the Rhône valley. The embedded convection inside the frontal perturbation was more active on 3 December. For that day, on which we will concentrate in the following, the upper level low-pressure area (Figure 4) associated with the surface cold front began to pivot slowly to a NW/SE axis and then stations over the Gulf of Lions area before progressing westward the last hours of the day. The observed precipitation maximum for that day was around 150 mm. Low-level winds also intensified during this day, with easterly wind gusts of 100–150 km h^{-1} on the French coasts. It resulted in a strong swell with beach-combers' waves of 9 m, disturbing the river water runoff to the sea.

[14] The exceptional character of this event lies in its spatial extent (approximately 25000 km^2 received more than 150 mm of precipitation), resulting in a major flood of the Rhône river (the Rhône's flow reached 13000 m^3/s). The flooding made 7 victims.

3. Experimental Design

3.1. MESO-NH Model

[15] The research nonhydrostatic mesoscale MESO-NH model's prognostic variables are the three components of the wind, the potential temperature, the turbulent kinetic energy and the mixing ratios of six water species (vapor, cloud water, rainwater, primary ice, graupel and snow) [*Lafore et al.*, 1998]. The prognostic equations of these latter are governed by a bulk microphysical scheme [*Caniaux et al.*, 1994; *Pinty and Jabouille*, 1998]. MESO-NH is run on two nested grids; the coarser grid provides the lateral boundary conditions to the finer grid meanwhile the variables of the coarser grid are relaxed toward the finer grid's values on the overlapping area. For the three cases, the coarser grid has a 9.5-km mesh and the finer grid a 2.4-km mesh. Figure 5 shows the domains used for each case. The vertical grid is defined by a stretched vertical coordinate [*Gal-Chen and Sommerville*, 1975]. It has 40 levels separated by 75 m in lower levels to 900 m for the highest levels. The first level is at 30 m while the model top is at 19 km. Rayleigh dumping is applied to the upper five kilometers of the model. For the coarser grid, the subgrid-scale convection is parameterized following *Bechtold et al.* [2001]. For the finer grid, no convection scheme is used. This model configuration has been already tested with success for simulation of Mediterranean intense rainfall events [*Ducrocq et al.*, 2002]. Note that the SST is prescribed at the beginning of the simulation and does not

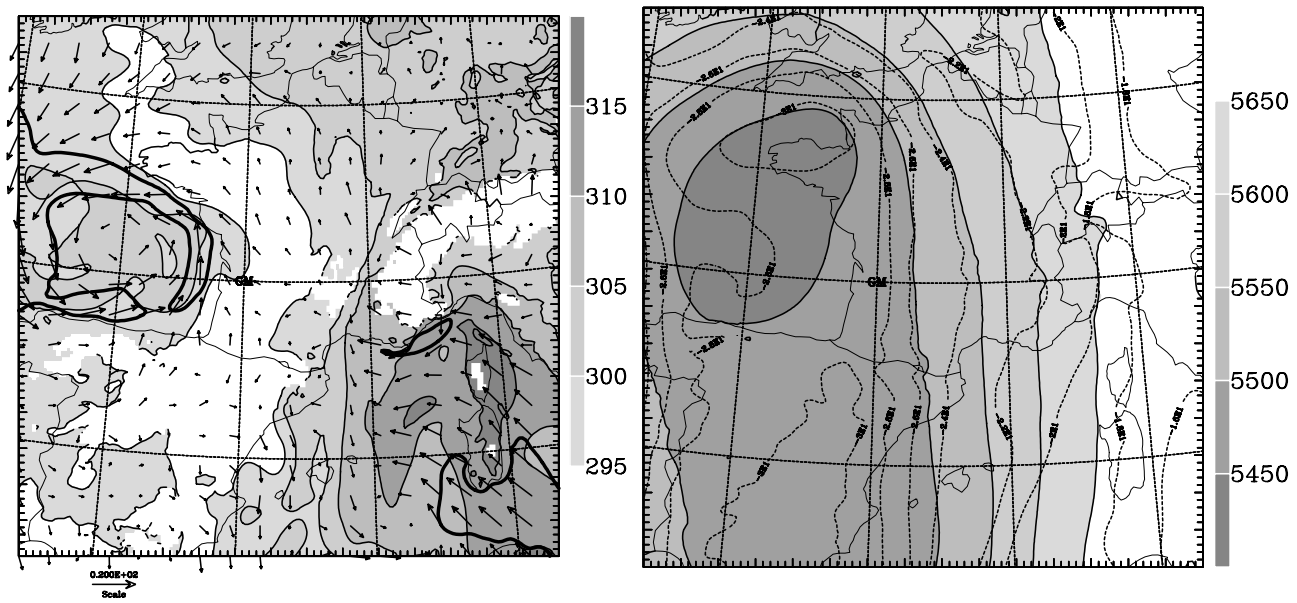

Figure 4. Hérault case: As in Figure 2 but at 0000 UT, 3 December 2003. The thick lines on the left plot delimit areas with wind superior to 12 m s^{-1}.

evolve during the short-range forecast, except for experiments with prognostic SST. We focus in the following on the results of the 2.4-km domain.

3.2. SST Data

[16] The initial SST fields used for the MESO-NH simulations are usually provided by the IFS or ARPEGE SST analysis. The ARPEGE SST analysis is obtained through an optimal interpolation which combines in situ data collected by ships and buoys with a first-guess analysis that is usually the previous 6-hour analysis but could also be the Reynolds global climatology at a $1^\circ \times 1^\circ$ resolution or the ECMWF SST analysis, when the former misses. The ARPEGE SST analysis error is estimated to about 1°C on average and can reach 2°C locally.

[17] Other products can also be used to prescribe the SST for the simulations. As an example, data are available four times a day from NOAA 16/17 Advanced Very High Resolution Radiometers (AVHRR) (at 0200 and 1200 UT for NOAA 16 and at 1000 and 2000 UT for NOAA 17) over a stereographic grid. Note that the SST data from NOAA 17 are predominant over the occidental Mediterranean basin. A high-quality data set derived from the NOAA polar-orbiting series of satellites is available since 1985. The multichannel SST product is derived from radiative temperatures of channels 4 and 5 in the infrared atmospheric windows at 3.5 μm, 11 μm and 12 μm [*McClain et al.*, 1985]. With the improvement of satellite and intersatellite calibration, quality control and cloud detection, the resolution of the SST products has increased. Missing data still however occur primarily because of the inability of the infrared sensors to access to the ocean temperature in cloudy regions. In the presence of cloud cover, SST data are obtained by a specific procedure using (1) a temporal collocation of one day

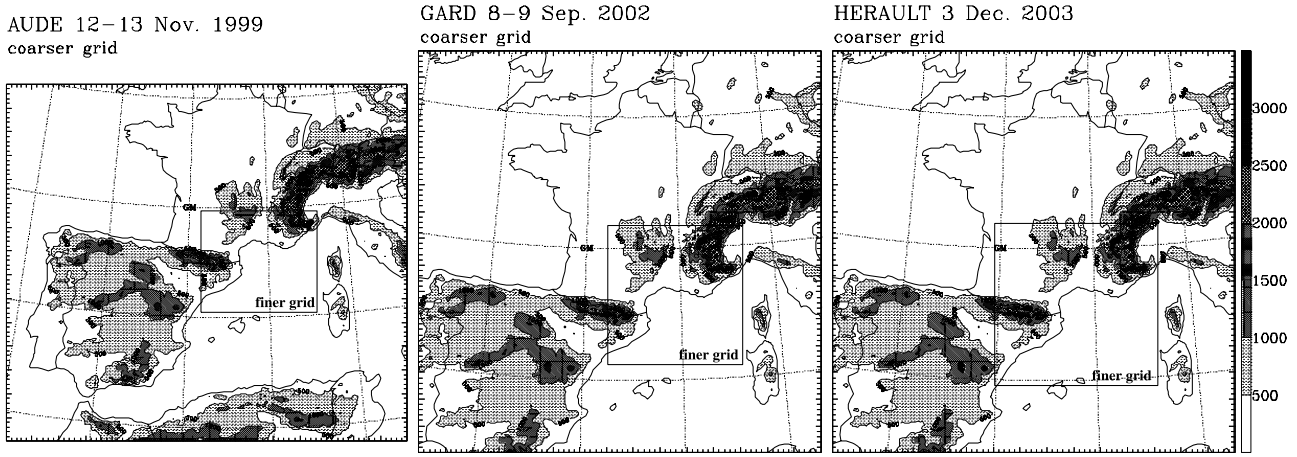

Figure 5. Model domains for simulations for the (left) Aude case, (middle) Gard case and (right) Hérault case. Orography (m) of the 9.5-km domain is shown in grey scale, and the box delineates for each case the 2.4-km domain.

Table 1. Numerical Simulations

	Aude Case	Gard Case	Hérault Case
Initial time	12 Nov 1999 1200 UT	8 Sep 2002 1200 UT	3 Dec 2003 0000 UT
Duration	18 Hours	24 Hours	24 Hours
	Simulations to Test Sensitivity to SST		
arphh			
SST field from ARPEGE analysis	arp12	arp12	arp00
noahh			
High-resolution SST with AVHRR data	noa12	noa12	noa00
stapX			
ARPEGE SST field	stap3	stap3	stap3
Increased by X°C	stap1.5	–	–
stamX			
ARPEGE SST field	stam1.5	–	–
Decreased by X°C	stam3	stam3	stam3
	Simulations With Prognostic SST		
evohh	evo12	evo12	evo00
Oceanic mixed layer depth, h (m)	27	10	35

around the current date for each four-daily measurements and (2) a spatial interpolation [*Ramos Buarque and Caniaux*, 2003]. The daily SST fields are finally filtered from the noise due to the data processing and are made available at a 2.5-km resolution.

[18] For a few years now, the Centre de Météo Spatiale (CMS) of Lannion in France produces operationally over a regular grid of 0.1° weekly SST analyses using AVHRR satellite data. Since recently, CMS produces operationally daily SST analyses using both AVHHR satellite data and in situ observations for the operational oceanographic model Mercator [*Bahurel et al.*, 2004]. SST data are available over a regular grid of 0.1° extending over the following area: 100°W, 45°E and 60°S, 60°N. The optimal analysis procedure assimilates all in situ data available over the domain and uses the previous analysis as guess. The standard deviation of analysis error ranges typically between 0.3°C and 0.5°C in the Mediterranean basin. For more details the reader is referred to *AVELMOR* [2002].

3.3. Numerical Experiments

3.3.1. Various SST Fields

[19] Different SST fields have been imposed as low-level boundary conditions over the Mediterranean basin. A first set of experiments, named arphh (Table 1) uses the SST from the ARPEGE analysis at the initial time (hh) of the simulation. It constitutes the reference experiment set. Simulations noahh use high-resolution satellite SST fields as described above for the Mediterranean Sea. For these experiments, the most up-to-date available product based on AVHRR has been used on each event. Finally, the SST fields have been obtained by increasing or decreasing uniformly the reference SST field. Indeed, for simulations named stapX, the SST field results from the ARPEGE analysis raised uniformly over the Mediterranean Sea by X°C. On the contrary, the ARPEGE analysis SST is lowered by X°C for simulations stamX. In a first set of simulations, X is set to 3°C in order to study the atmospheric response to extreme anomalies of SST; in a second set, X is set to an intermediary value 1.5°C.

[20] For the Aude case, all the simulations start at 1200 UT, 12 November 1999, and last for 18 hours. Atmospheric initial conditions are provided by the ARPEGE analysis (Table 1). The SST field of the control simulation arp12 exhibits a north-south gradient over the Mediterranean Sea, with coldest values near the French coasts (Figure 6). The mean SST value over the finer MESO-NH domain is about 18°C (Table 2). The simulation noa12 uses a weekly Mediterranean SST analysis at a 10-km resolution based on AVHRR/NOAA data. This SST field exhibits finer-scale structures than the ARPEGE one, with a cold anomaly in the Gulf of Lions (Figure 6). The satellite SST is also warmer near the littoral and to the west of Corsica. On the average, the satellite SST is colder than the ARPEGE one, with a bias of about 0.4°C over the finer domain (Table 2).

[21] For the Gard flash-flood case, all the simulations are initialized at 1200 UT, 8 September 2002, from the ARPEGE analysis and last for 24 hours (Table 1). The reference simulation arp12 uses the ARPEGE SST analysis, which presents a north-south gradient with the coldest values over the Gulf of Lions (Figure 7). The noa12 simulation uses the daily AVHRR SST at 2.5 km dated 8 September 2002. SST satellite field shows finer-scale structures than the ARPEGE SST one and a stronger north-south gradient (Figure 7). On average, the SST field is warmer than the ARPEGE one (Table 2).

[22] For the Hérault case, all the simulations start from the ARPEGE analysis at 0000 UT, 3 December 2003, and last for 24 hours (Table 1). The ARPEGE SST analysis is used for the reference simulation arp00. For this case, a daily Mediterranean SST field analyzed for the ocean forecasting Mercator system is available and has been used for noa00. The coldest values in the high-resolution SST field are located near the Rhône delta and over the Gulf of Lions (Figure 8). Differences from the ARPEGE SST analysis reach more than +2°C in the Gulf of Genoa and near the extreme east coasts of France, but on average satellite SST is slightly colder than the ARPEGE one.

3.3.2. Prognostic SST

[23] For the evohh simulations (Table 1), the SST is allowed to evolve during the model integration. Its evolution is governed by the heat balance at the sea-atmosphere interface following *Gaspar* [1988]. It can be considered as a

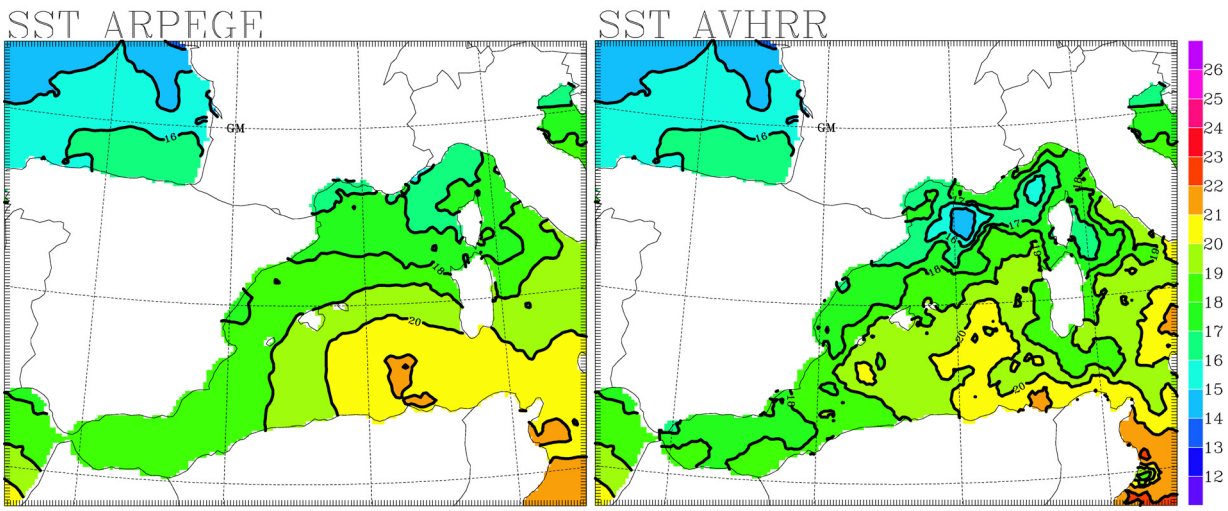

Figure 6. ARPEGE SST and AVHRR SST fields (in °C) for the Aude case interpolated on a zoom of the coarser MESO-NH grid.

basic coupling between the upper layers of the ocean and the atmosphere. The superficial ocean or oceanic mixed layer is considered as a homogeneous layer of depth h and its temperature is equal to the SST. In a first approach, (1) h is kept constant in space and time and deduced from the mean value of the *Levitus* [1982] monthly climatology on the Mediterranean Sea and (2) no entrainment/detrainment processes at the bottom of the mixed layer and no advection are taken into account. On the basis of these hypotheses, the prognostic equation for the SST introduced in the MESO-NH model is

$$\frac{\partial SST}{\partial t} = \frac{R_N - LE - H}{\rho c_p h} \tag{1}$$

where ρ is the volumetric mass of seawater, c_p the calorific capacity of water, and R_N, LE and H are the net radiation, the latent heat and the sensible heat surface fluxes, respectively (the MESO-NH equations of the sea surface fluxes are given in Appendix A). h is the oceanic mixed layer depth previously defined; Values chosen for h are given in Table 1.

3.3.3. Evaluation Methodology

[24] In order to analyze the simulation results, the following questions are addressed:

[25] 1. How much the simulation of the convection is modified? It is achieved by examining the accumulated surface rainfall, the synthetic radiances and reflectivity field.

[26] 2. How the environment is made more or less propitious to convective developments? This can be assessed through examination of CAPE, precipitable water and low-level jet fields for example.

[27] 3. How the low-level conditions are altered through the modifications of the air-sea interface fluxes?

[28] In order to perform a more objective comparison between simulations, we also used integrated parameters, such as averaged parameters (surface fluxes, hydrometeor contents, etc.) over regions of the finer domain computed at a 1-min step during the model integration. We also score the simulations with respect to the reference experiment on each case.

4. Results

4.1. Reference Simulations

[29] For the two cases of quasi-stationary MCS (Aude and Gard cases), the reference experiments (arp12) succeed in simulating well-developed and quasi-stationary convective systems. Whereas the simulated MCS's localization is close to the observed one for the Aude flash-flood (Figure 9), the simulation for the Gard case places the maximum of precipitation over the Cévennes relief, about 80 km northwest of the observed maximum (Figure 10). Different initialization time (0000 or 0600 UT) using ARPEGE analysis leads to the same drawback. A better localization of the precipitation maximum can be obtained by applying a mesoscale data analysis to produce the initial conditions [*Ducrocq et al.*, 2000, 2004]. However, in order to have the same experimental framework for the three cases allowing intercomparison, we have chosen here to start all the simulations from an ARPEGE analysis. Note, however, that the simulation of the Gard case places the precipitation maximum over a region that is typically affected by these types of events. Therefore the simulated rainfall episode can be nonetheless considered as representative of torrential events occurring in this area.

[30] For the Hérault case, arp00 catches almost perfectly the frontal system extended over the Gulf of Lions and the associated strong low-level winds convergence. Since the

Table 2. Averaged Values of the Mediterranean SST (°C) Both for the 9.5-km Domain (D1) and the 2.4-km Domain (D2)

	Aude Case		Gard Case		Hérault Case	
	D1	D2	D1	D2	D1	D2
arphh	19.0	17.8	23.6	22.1	17.0	16.5
noahh	18.8	17.4	24.5	23.2	16.8	16.2

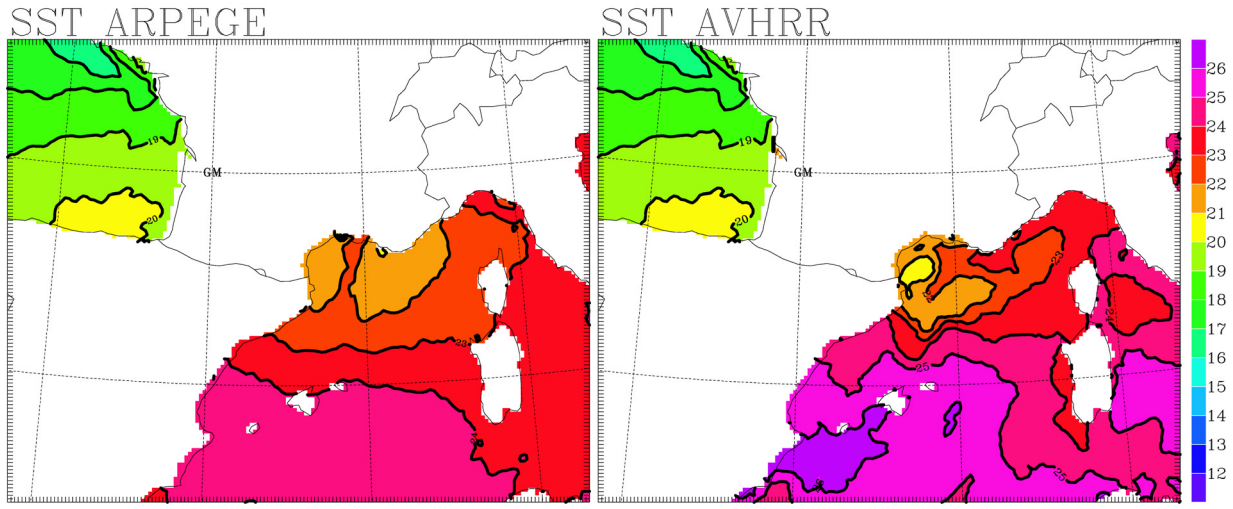

Figure 7. As in Figure 6 but for the Gard case.

front progresses a little slower during the afternoon than in the observations, simulated rainfall totals are weakly overestimated compared to those observed over land (Figure 11): The observed rainfall maxima in 24 hours are between 150 and 200 mm over land, whereas those simulated reach 220 mm. Note that the absolute maximum of simulated precipitation occurs over the Mediterranean Sea (343 mm, Figure 12) where no observation is available for the validation.

[31] Thanks to their high-resolution, allowing an explicit resolution of convection, and to more advanced parameterizations, the reference simulations produce larger precipitation than those produced by the actual operational models, but still underestimated compared to the observed maxima for the Aude and Gard cases. For example, the rainfall maximum accumulated during 18 hours reaches about 300 mm for the Aude case whereas the observations indicate maximum values above 480 mm. Nevertheless, this value is twice more important than those produced by the current operational models [*Ducrocq et al.*, 2004].

[32] The meteorological environments simulated by the reference contain the typical ingredients needed for a convective systems development. For example, for the Aude case, the simulation reproduces an environment propitious to convection: Figure 13a shows the temporal evolution of sensible and latent heat fluxes averaged over the 2.4-km domain. After a time of adjustment during the first hours of simulation, the mean latent heat flux stays almost around 200 W m^{-2} which is a relatively high value; the sensible heat flux is weaker with a mean value of -4 W m^{-2}. The strongest values of surface heat fluxes (more than 500 W m^{-2}) are simulated in association with the strong southeasterly and easterly low-level jets converging over the Gulf of Lions and related to both the deflection of the flow by the Alps and the synoptic forcing (Figure 14). The southeasterly low-level jet is associated with a moist and unstable tongue, with CAPE values reaching about 2000 J kg^{-1}.

[33] The simulation for the Gard case produces also an intense southerly low-level jet (Figure 15) associated with high precipitable water and CAPE values. Latent and sensible heat fluxes are weaker than those simulated on

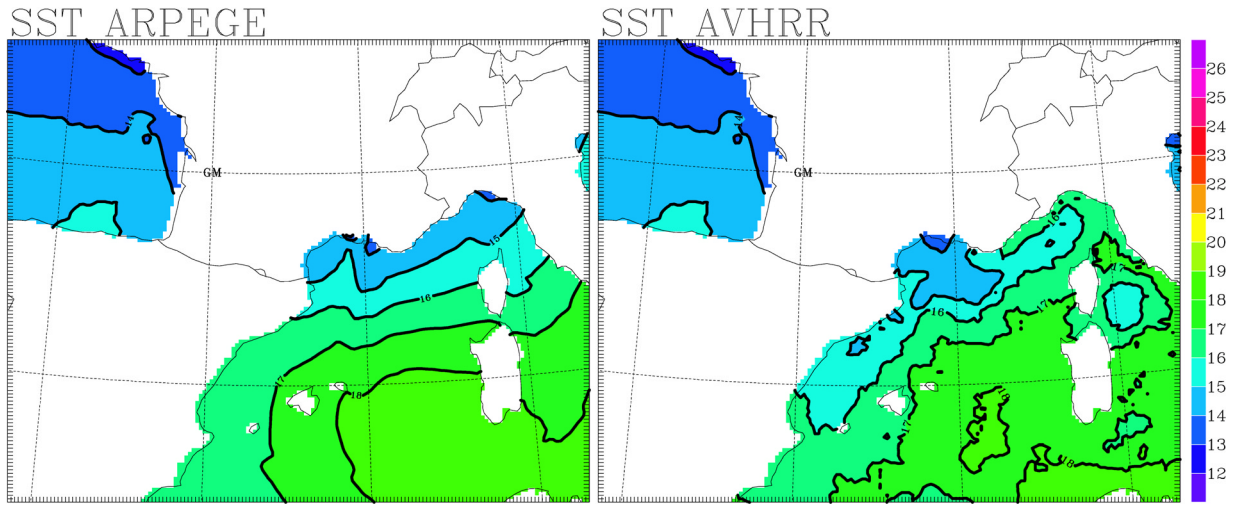

Figure 8. As in Figure 6 but for the Hérault case.

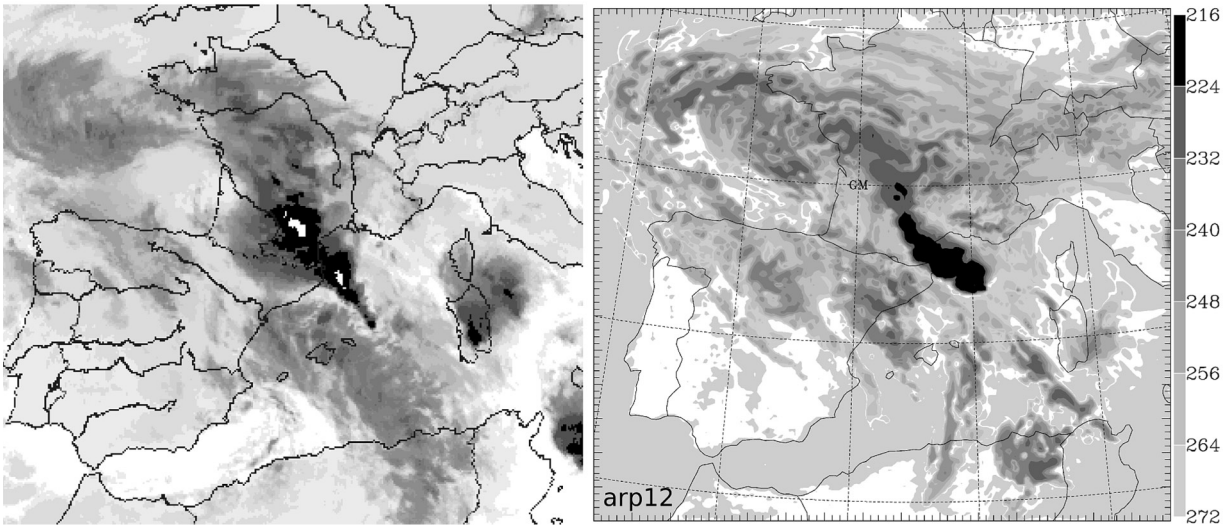

Figure 9. Infrared radiances (K) for the Aude case at 0300 UT, 13 November 1999: (left) observed from METEOSAT and (right) synthetic radiances from arp12.

the Aude case, with average values over the sea around 70 W m^{-2} and -11 W m^{-2}, respectively, for all the duration of the simulation (Figure 13b).

[34] For the Hérault case, intense southeasterly winds are simulated (Figure 16) and the area of maximum wind speed progressed westward with the surface front. It results in an increase of the latent and sensible heat fluxes over the 2.4-km domain after midnight (Figure 13c). On average during the 24 hours of simulation, the latent heat flux over the sea is 80 W m^{-2} and the sensible heat flux 9 W m^{-2}.

4.2. High-Resolution SST

[35] Experiment noa12 produces convection almost as intense as in arp12; The 18-hour rainfall totals are only slightly weaker (Table 3) with a maximum reaching 296 mm against 303 mm for arp12 (Figure 12). As for arp12, the location of this maximum is very close to the observed one. Figure 17a shows the temporal evolution of the precipitating hydrometeors averaged on a 3D box including the convective system. After 3 hours of simulation, the graupel content in noa12 begins to be slightly lower than the arp12 one and remains lower for the rest of the simulation; this is related to weaker vertical velocities inside the convective cells. Concerning the rainwater and snow contents, there is no significant difference between noa12 and arp12 for the first 10 hours and 13 hours of simulation, respectively. The environment of the convection is also characterized by a slightly weaker convective conditional instability during the first 12 hours of simulation (Table 3). No significant difference is found for the precipitable water as well as for the low-level jet. Whereas low-level fields of prognostic model variables (wind, temperature, etc.) do not exhibit a

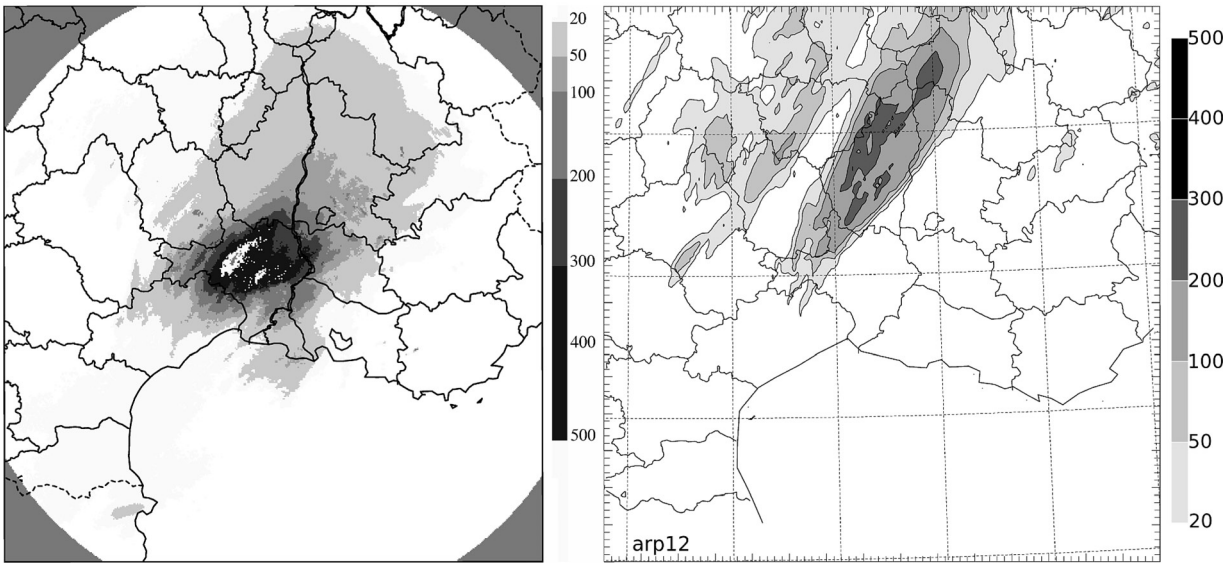

Figure 10. Twenty-four-hour accumulated precipitation (mm) at 1200 UT, 9 September 2002, for the Gard flash flood case: (left) from radar and (right) from arp12 simulation.

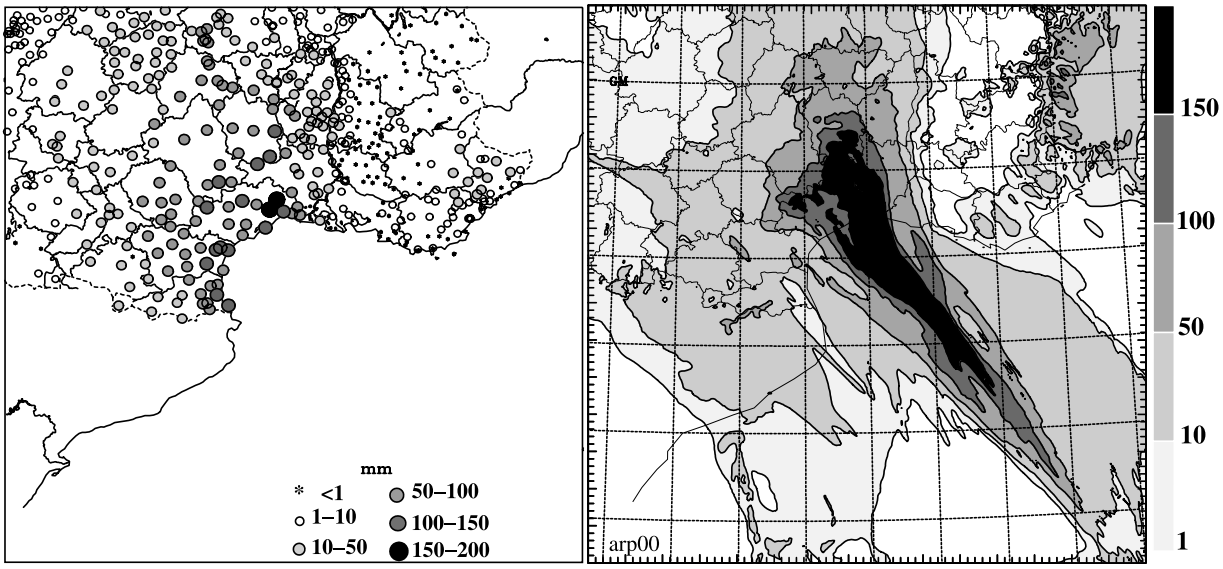

Figure 11. Twenty-four-hour accumulated precipitation (mm) at 0000 UT, 4 December 2003, for the Hérault case: (left) from rain gauges and (right) from arp00 simulation.

signature related to the cold SST mesoscale anomaly, heat surface fluxes clearly show a direct response to it and more generally to the mesoscale structures of the satellite SST field (not shown). Simulated surface heat fluxes are larger near the coasts where the satellite SST is warmer than the ARPEGE SST. On the contrary above the cold SST anomaly, they are clearly weaker (not shown). Sensible and latent heat fluxes values above the specific area of this cold SST anomaly reach on averaged -120 W m^{-2} and -50 W m^{-2}, respectively, whereas the corresponding values for arp12 at the same location were -50 W m^{-2} and 50 W m^{-2}, respectively.

[36] For the Gard case, slightly larger rainfall totals are produce by noa12 with respect to arp12; the accumulated rainfall maximum after 24 hours is of 322 mm (19 mm more than arp12, Figure 12). The pattern of rainfall totals is slightly modified in noa12 (compare Figures 10 and 18). Concerning precipitating species (Figure 17b), some departures between noa12 and arp12 are discernible after about 10 hours of simulation, with a higher mean content for noa12. Warmer SST results in higher precipitable water and larger CAPE (Table 3), according to slightly more intense convection. Nonetheless, there is almost no difference in the low-level wind field. Again, the fine scale structures of the satellite SST field influence sea surface heat flux patterns, whereas no similar fine-scale structures are found for the other atmospheric boundary layer fields.

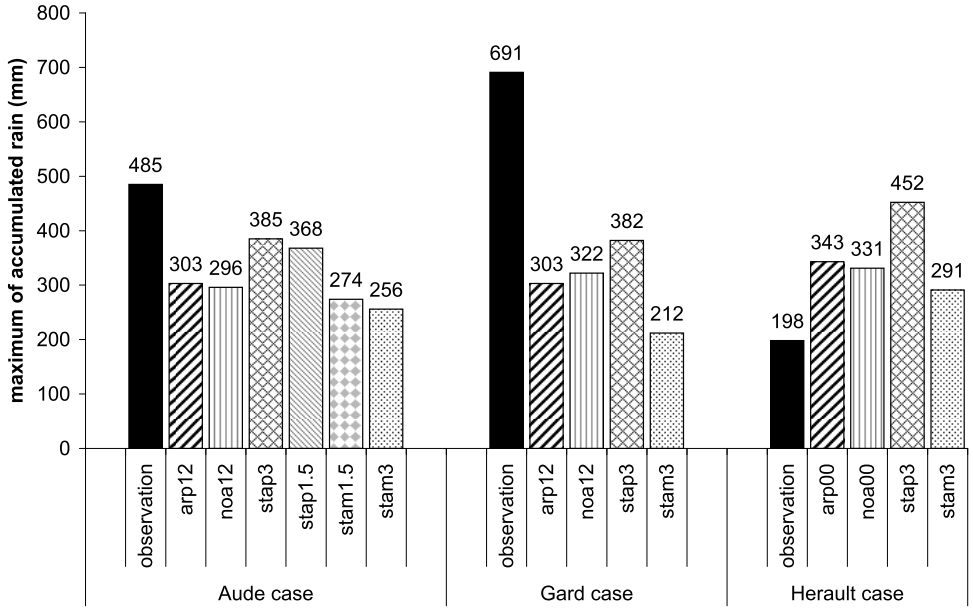

Figure 12. Maximum accumulated surface rainfall observed and simulated (mm). See Table 1 for simulation names and periods of accumulation (i.e., the total simulation duration).

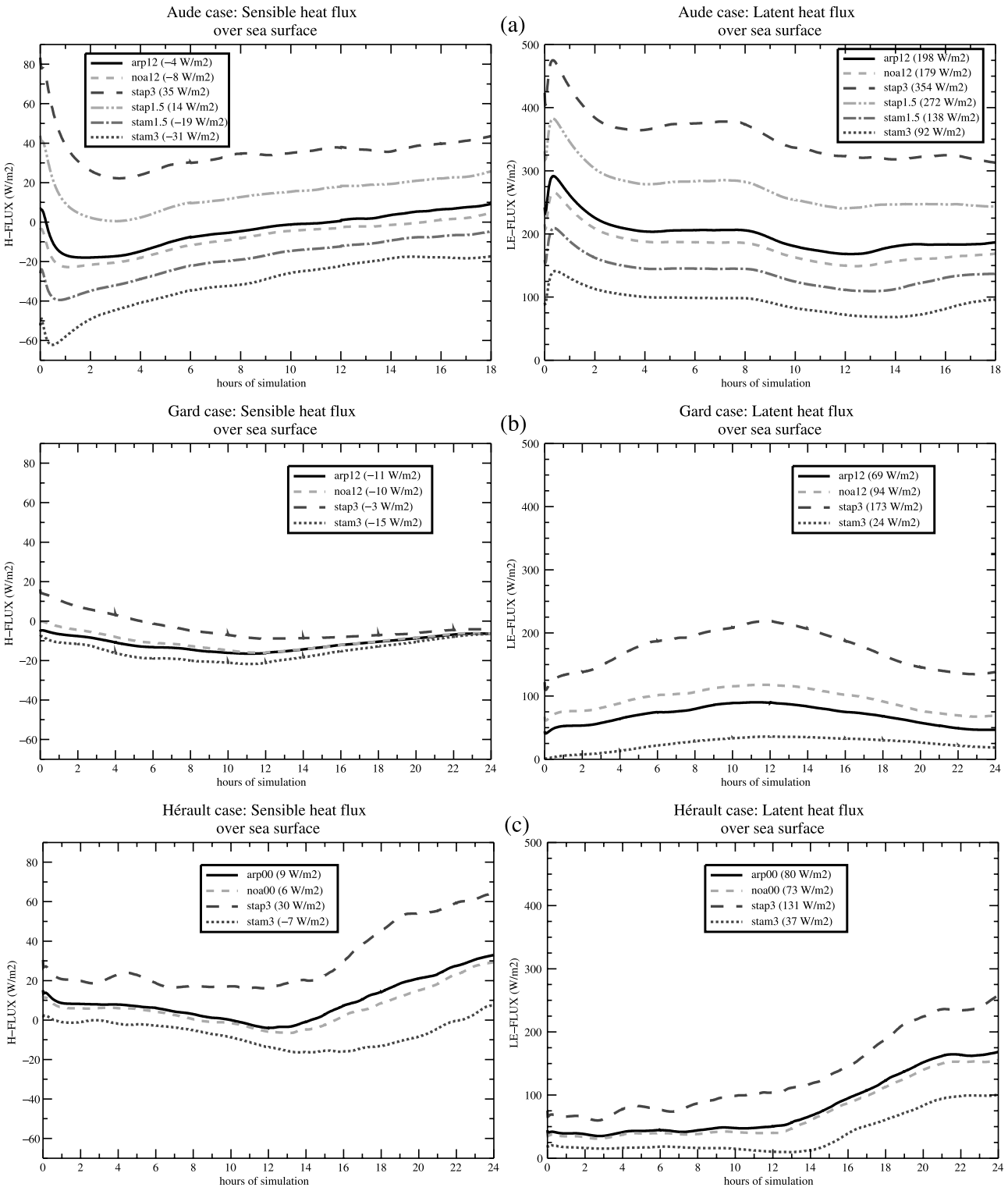

Figure 13. Temporal evolution of sensible (H-FLUX) and latent (LE-FLUX) heat fluxes (W m^{-2}), averaged over sea grid points of the 2.4-km domain (a) for the Aude case, (b) for the Gard case and (c) for the Hérault case. The averaged values for the total duration of the simulations are indicated in parentheses.

[37] For the Hérault case, there are almost no difference between the precipitation location forecast. The bias in term 24-hour accumulated rainfall is only −0.1 mm (Table 3) and the maximum value is slightly decreased (Figure 12). As for the two other cases, latent and sensible heat fluxes are the most sensitive to the fine scale structures of the SST and more particularly under the low-level jet (not shown). For example, near the outermost southeastern coasts of France,

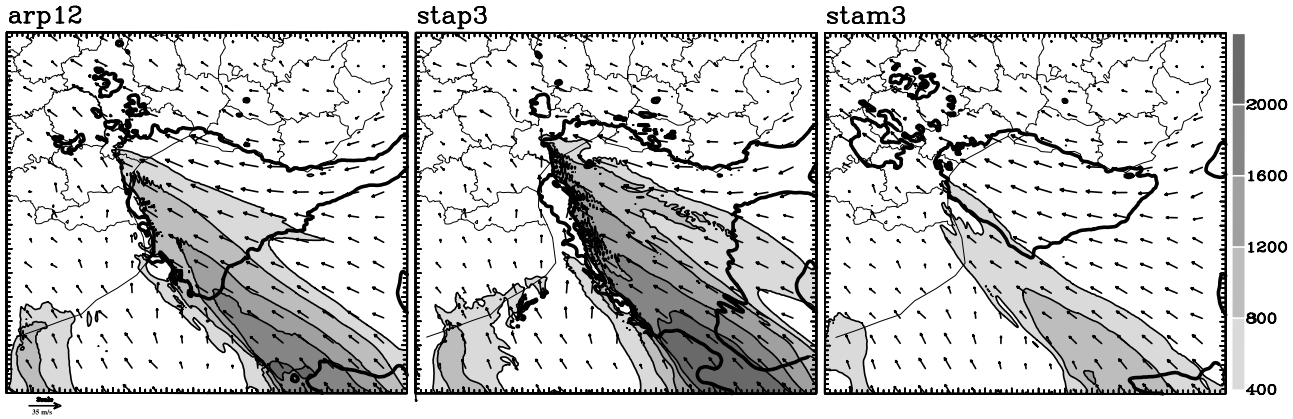

Figure 14. Aude case: CAPE (grey scale in J kg^{-1}) and 30-m AGL horizontal wind vectors at 0000 UT, 13 November 1999. The wind vectors are drawn every two grid points with the unit vector length shown at the bottom left corner corresponding to 35 m s^{-1}. The thick lines delineate areas with wind greater than 15 m s^{-1}.

where the high-resolution satellite SST is warmer, the sensible and latent heat fluxes at 0000 UT, 4 December, are increased by 50 W m^{-2} and by more than 120 W m^{-2}, respectively (not shown). On the contrary, over the Gulf of Lions, where the high-resolution SST is colder than the ARPEGE one, heat surface fluxes are decreased by approximately the same amounts. It is worth pointing out that the response of heat surface fluxes to SST anomalies is strongly linked to the strength of the low-level winds. For example, whereas the SST is colder in noa00 than in arp00 along the Spanish coast, there is no difference between the heat surface fluxes of noa00 and those of arp00 the latter being characterized by weaker low-level winds in this area.

[38] Results of the noahh experiments show that when the high-resolution satellite SST is in average colder (warmer) over the Mediterranean Sea than the ARPEGE SST, then the convection is less (more) intense. At variance with the sea surface heat fluxes, the precipitating systems are not very sensitive to the finer-scale patterns and stronger SST gradients that are present in the high-resolution SST fields. Consequently, regarding the high-resolution Quantitative Precipitation Forecast (QPF), the controlling factor seems to be rather the mean SST over the basin than the mesoscale patterns of the SST fields. Consequently, for the next operational high-resolution short-range NWP forecast systems, SST products at coarser resolution without significant mean bias error over the western Mediterranean basin (typically less than 0.5°C) appear to be sufficient according to these sensitivity tests.

4.3. Raised/Lowered SST

[39] The responses of the studied convective systems to large modifications of analyzed SST fields are investigated in this section. The ARPEGE SST fields are raised or lowered uniformly over the Mediterranean Sea.

[40] For the Aude case, when the SST is raised by 3°C over the Mediterranean Sea (stap3, Table 1), the convection is considerably intensified. Indeed, the 18-hour accumulated rainfall bias is on average 5 mm larger than in arp12 (Table 3). The precipitation maximum is 385 mm (i.e., 82 mm more than in arp12, Figure 12) and it is located northeast of the arp12 maximum. This displacement can be

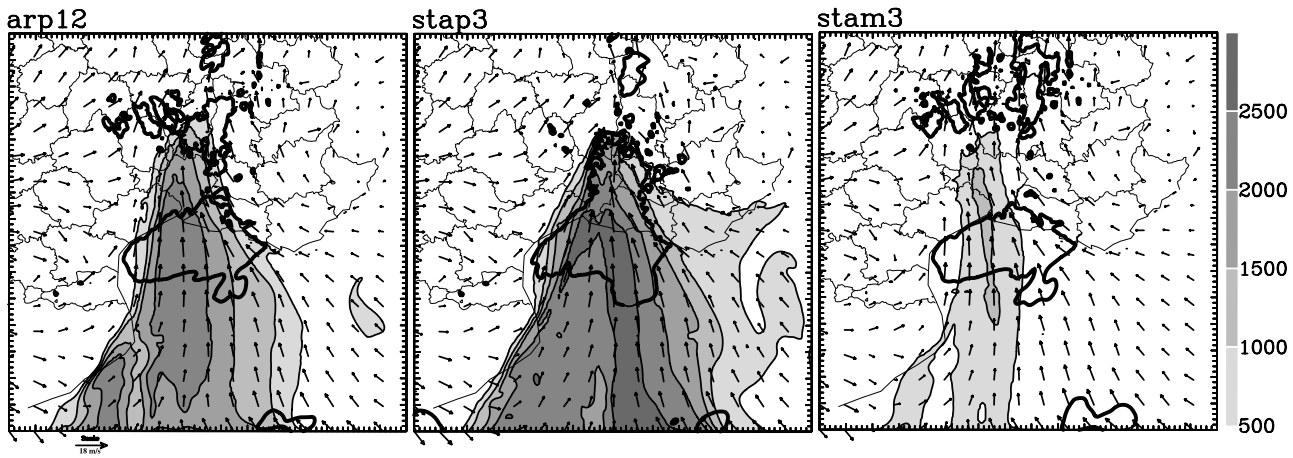

Figure 15. Gard case: As in Figure 14 but at 0600 UT, 9 September 2002. The unit vector length shown at the bottom left corner corresponds to 18 m s^{-1}. The thick lines delineate areas with wind greater than 10 m s^{-1}.

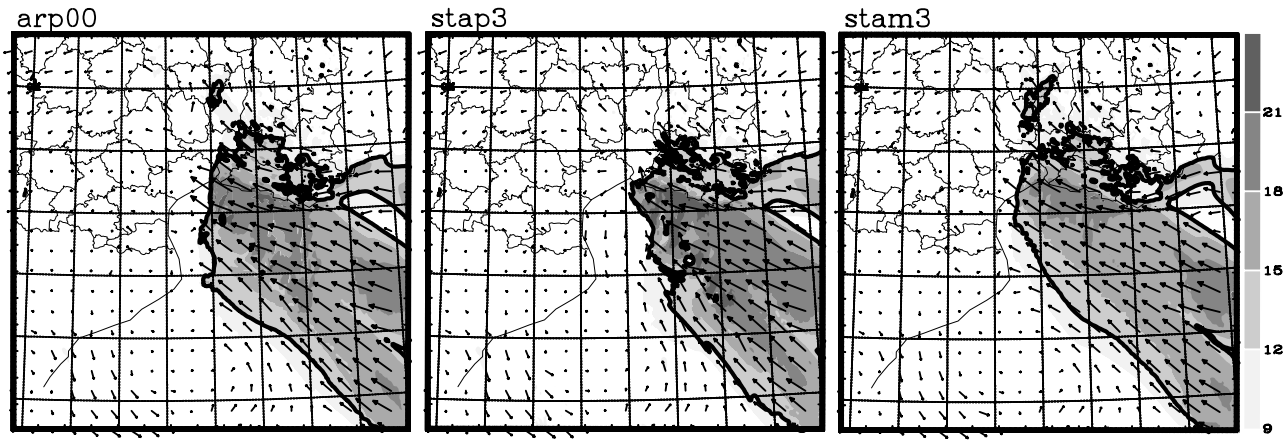

Figure 16. Hérault case: 30-m AGL horizontal wind (grey scale in m s^{-1}) at 1200 UT, 3 December 2003. The thick lines delineate areas with wind greater than 12 m s^{-1}.

partly explained by a faster eastward progress of the MCS: The low-level convergence zone and the conditional instability tongue that sustains the convection move more quickly eastward (Figure 14). Figure 19 shows the vertical profile of θ_e averaged over the sea. Larger values are simulated in stap3 in the lower levels as a consequence of the warmer sea. In the middle and upper troposphere, the warming of θ_e is due to the moistening and latent heat release. The convection intensity is also more important with also a wider area over sea concerned by convection. Vertical velocities inside the convective system reach larger values than in arp12, resulting in a significant increase of the graupel content in the convective areas, almost twice the values of arp12 at 0300 UT, 13 November 1999 (Figure 17a). Rainwater and snow contents are also larger. Departures between stap3 and arp12 hydrometeor contents begin as soon as the simulation has run only a few hours. From the beginning of stap3, latent and sensible heat fluxes, in particular under the low-level jet, are significantly larger (Table 3). The initial adjustment is slightly longer in time for the sensible heat flux, but afterward heat fluxes averaged over the sea have the same temporal evolution as those of arp12, with a significant positive shift (Figure 13a).

[41] When the SST is lowered by 3°C (stam3), latent and sensible heat fluxes become weaker under the low-level jet (Figure 13a), becoming more homogeneous over the Gulf of Lions. The atmosphere is less unstable (Table 3) and less moist than in arp12. After several hours of simulation the convective activity decreases in stam3. The cloud tops do not reach any more the tropopause level. The graupel content is significantly decreased whereas the snow content is only slightly reduced (Figure 17a). It results in more spreading stratiform precipitation, with only few embedded convective cells. The maximum of 18-hour accumulated rainfall is about 50 mm less than in arp12 (Figure 12). At the end of the simulation, the MCS moves eastward less rapidly than in arp12. The low-level jet decreases clearly in intensity during the 18 hours of simulation (Figure 14).

[42] When the SST is raised (lowered) by only 1.5°C, results are intermediate between those from stap3 (stam3) and arp12 (Table 3). For example, the accumulated rainfall maximum for stap1.5 reaches 368 mm after 18 hours of simulation (Figure 12) and the maximum value of CAPE is increased by 190 J kg^{-1} compared to arp12 and decreased of 260 J kg^{-1} compared to stap3. In simulation stam1.5, sensible and latent heat fluxes are on average weaker than in arp12 (Figure 13a). The warm and unstable air supplied to

Table 3. Bias and RMS Errors From the Reference Experiment for the Aude Case, the Gard Case and the Hérault Case Computed Over the 2.4-km Domain at the End of Simulation (After 18 Hours of Simulation for the Aude Case and After 24 Hours for the Gard and Hérault Cases)

	Aude Case					Gard Case			Hérault Case		
	noa12	stap3	stap1.5	stam1.5	stam3	noa12	stap3	stam3	noa00	stap3	stam3
Accumulated precipitation, mm											
Bias	−0.9	4.9	2.5	−2.1	−3.7	1.7	5.7	−3.4	−0.1	4.1	−3.2
RMS	9.9	29.9	17.9	16.9	20.6	12.6	31.2	19.3	10.5	47.9	25.8
CAPE, J kg^{-1}											
Bias	2.5	84.9	58.5	−60.2	−128.3	77.4	168.3	−377.1	−5.9	34.0	−16.4
RMS	102.5	286.9	197.0	170.0	260.1	300.7	769.0	715.8	25.4	73.4	41.4
Latent heat flux over sea, W m^{-2}											
Bias	−9.5	68.8	31.0	−27.1	−49.6	11.4	47.1	−16.2	−3.8	59.3	−47.7
RMS	39.3	109.5	53.3	45.0	75.6	24.9	74.1	27.2	24.8	84.7	68.5
Precipitable water, kg m^{-2}											
Bias	0.07	0.36	0.25	−0.16	−0.36	0.38	0.99	−1.04	−0.09	0.49	−0.38
RMS	0.57	1.23	0.91	0.75	0.94	1.43	3.25	2.21	0.39	0.96	0.73

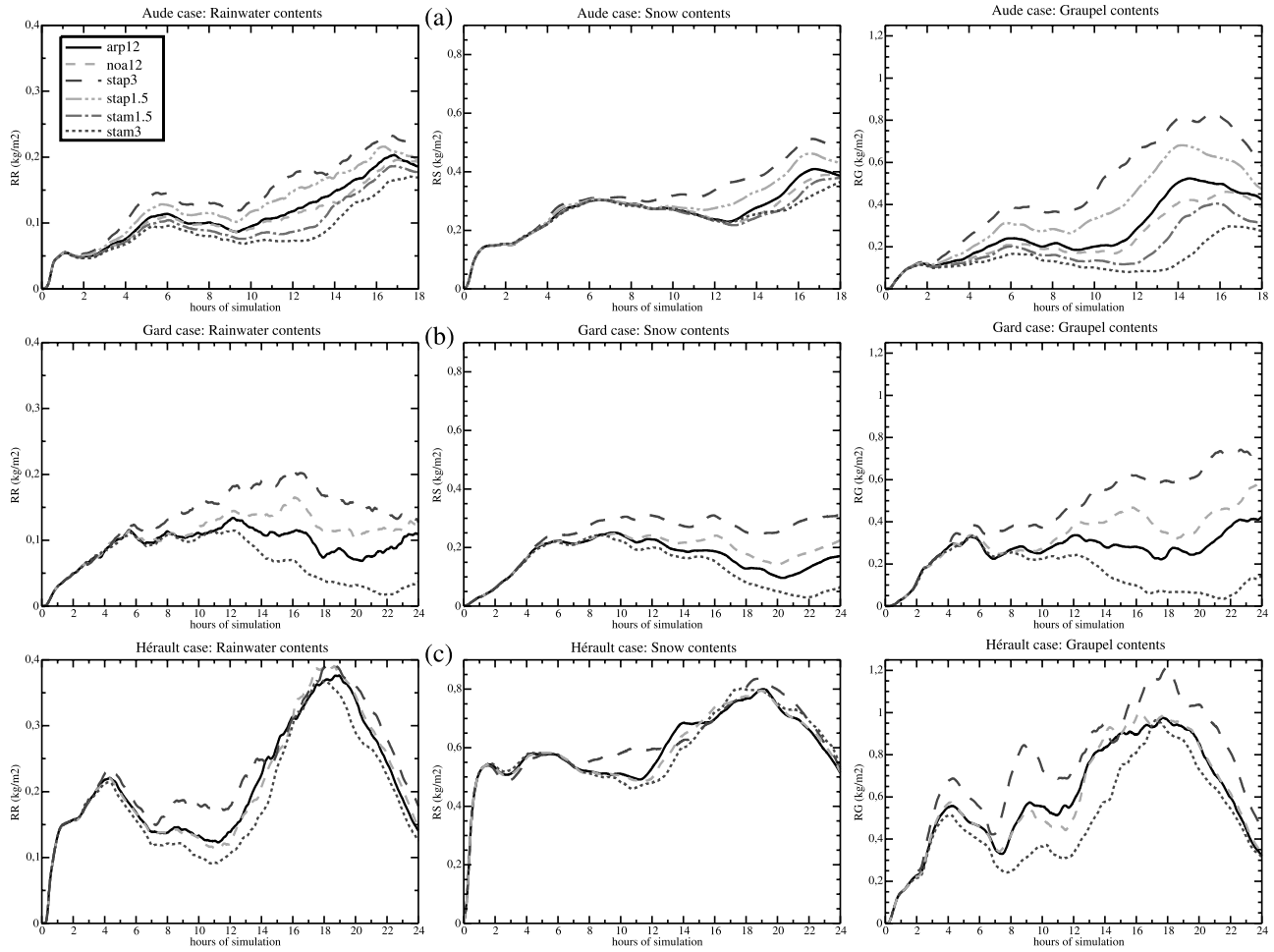

Figure 17. Time series of rainwater (left column), snow (middle column) and graupel (right column) contents in kg m^{-2} from all the simulations, for (a) the Aude case, (b) the Gard case and (c) the Hérault case. The content is averaged on a 3D box including the precipitating system for each case.

the MCS is less broad and less intense (Table 3). Stratiform precipitation still dominates, but embedded convective activity is less reduced than in stam3.

[43] On the basis of the fact that the simulated responses of the convection and of low-level jets to an increase (decrease) of 1.5°C are intermediate between those obtained with arp12 and stap3 (stam3) for the Aude case, we only examine in the following the sensitivity of the high-resolution simulations to an increase (decrease) of 3°C for the two other cases.

[44] For the Gard case, results concerning with hydrometeor content show that after nearly 4 hours of simulation, stam3 and stap3 deviate from arp12 (Figure 17b). Whereas the upper circulation is unchanged, the SST field has a significant impact on the simulation of the MCS in terms of intensity, motion and extension of its cold pool. When the SST is raised (lowered) by 3°C, the convective precipitation of the MCS is located more southward (northward). Moreover, the MCS and the frontal system move faster to the east in stap3, resulting in a more widespread rainy area (compared the 24-hour accumulated precipitation in Figures 10 and 18). The 24-hour accumulated rainfall maximum is 79 mm more than in arp12 (Figure 12). On the opposite, the maximum of 24-hour accumulated rainfall simulated by stam3 is reduced by 91 mm (Figure 12). The deep convection vanishes with time in stam3, being replaced by shallow orographic convection over the Cévennes-Vivarais range. This is obvious analyzing on the temporal evolution of the graupel content, which decreases after 12 hours of simulation (Figure 17b). The cold pool beneath the storm is also weaker before completely disappears after a few hours of simulation.

[45] Some impacts are also visible on the low-level jet feeding the MCS in conditional unstable air. Its intensity is decreased in stam3 whereas it is reinforced in stap3 (Figure 15). The mean vertical profiles of θ_e over sea (Figure 19) show that the increase of SST moistens and warms the atmosphere up to about 2000 m, resulting in larger CAPE and precipitable water (Table 3). Note that, since there is no convection over the sea for the Gard case, there is almost no difference in mid to upper levels for the θ_e mean profiles. The latent heat fluxes are increased on average by 100 W m^{-2} (Figure 13b). On the opposite, the decrease of SST produces a less unstable mean vertical profile. This results mainly from weaker latent heat fluxes over the Mediterranean Sea which are reduced by about 50 W m^{-2} on average in stam3 compared to those of arp12 (Figure 13b). As in the Aude case, it is worth to note that the

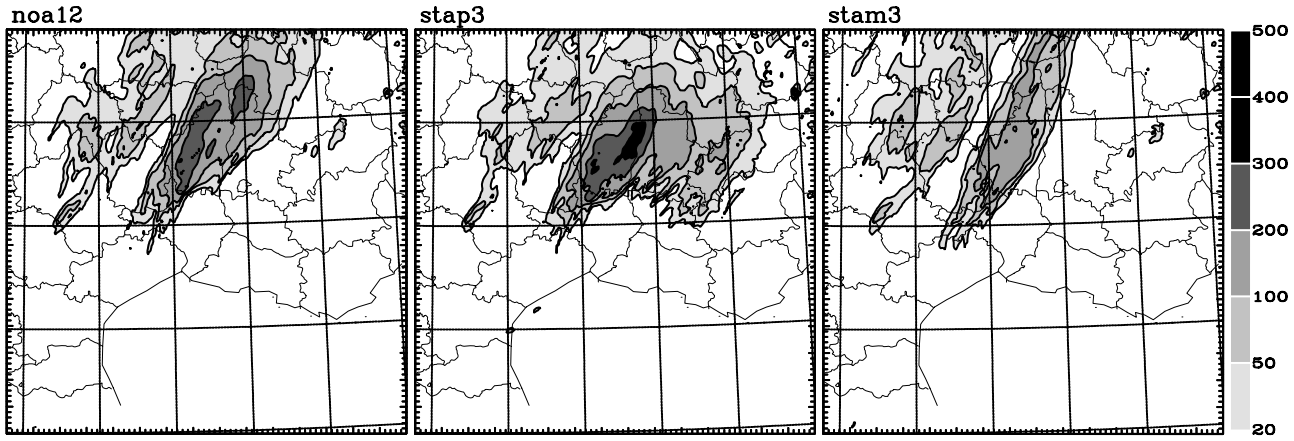

Figure 18. Twenty-four-hour accumulated precipitation (mm) simulated at 1200 UT, 9 September 2002, for the Gard flash flood case, for (left) noa12, (center) stap3 and (right) stam3.

sensitivity to a +3°C or a −3°C variation is not symmetric with respect to the reference simulation: the gap between stap3 and arp12 curves is larger than the gap between arp12 and stam3 curves. The nonsymmetry of the sea surface fluxes can be related to their formulation (Appendix A): the exponential form of the Clausius-Clapeyron relationship used for the saturated specific humidity and the dependence of the heat transfer coefficient on the thermal stability induced a nonsymmetric response to the SST. The diabatic processes associated with the convection could also undergo a nonlinear response to the SST forcing.

[46] For the Hérault case, as for the two other cases, atmospheric low levels are more (less) warmed and moistened when the ARPEGE SST is increased (decreased), according to increase (decrease) of surface heat fluxes at the air-sea interface (Table 3 and Figure 13c). The influence of the SST is visible up to nearly 3000 m on the mean θ_e profile over sea surface after 15 hours of simulation (Figure 19). Rainfall totals, CAPE and precipitable water are increased (decreased) in stap3 (stam3) compared to the reference simulation (Table 3).

[47] The impact on the dynamics for the Hérault case is more complex than for the two other cases. In the first phase of the event, when the north-south elongated frontal system moves westward, the embedded convection associated with the frontal perturbation is more active in stap3. Consequently, the westward progression of the precipitation system is slowed down (Figure 16). On the opposite, with stam3, the embedded convection almost disappears, allowing a more rapid westward progression of the rainfall system. In the second phase of the event, when the frontal system takes progressively a NW/SE orientation in association with the upper level dynamic forcing, the differences between experiments reduce. Stronger low-level wind convergence at the front surface is however produced by stap3 because of more intense convective activity inside the front. Increasing

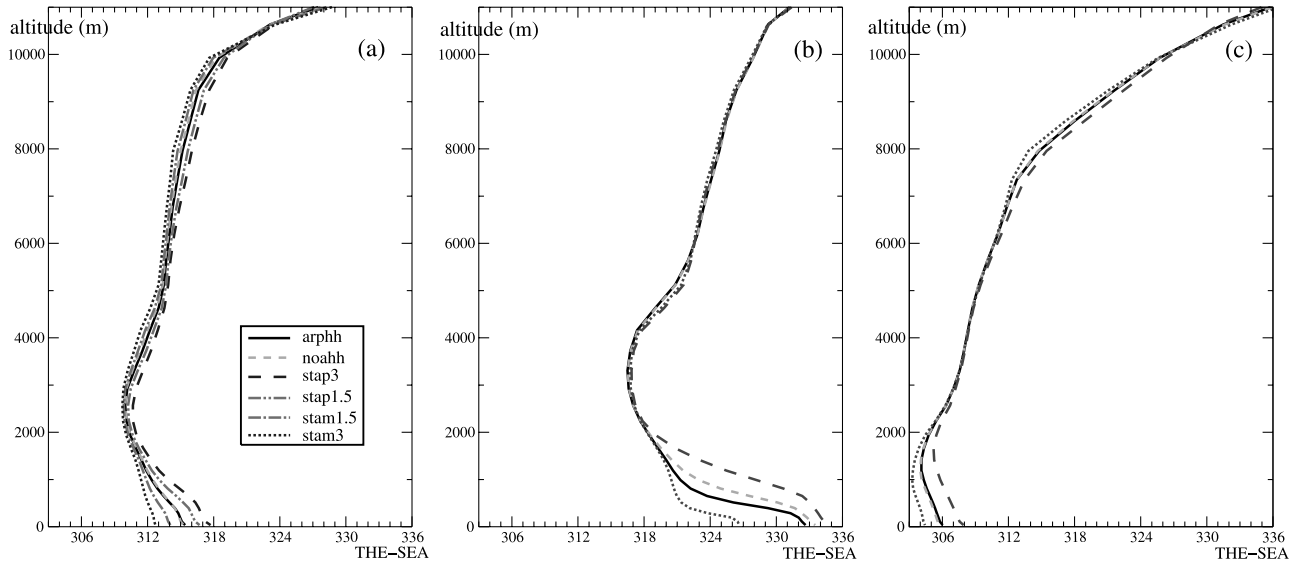

Figure 19. Vertical profiles of equivalent potential temperature (K) averaged over sea surface on the 2.4-km grid for all the simulations: (a) for the Aude case at 0300 UT, 13 November 1999; (b) the Gard case at 0300 UT, 9 September 2002; and (c) the Hérault case at 1500 UT, 3 December 2003.

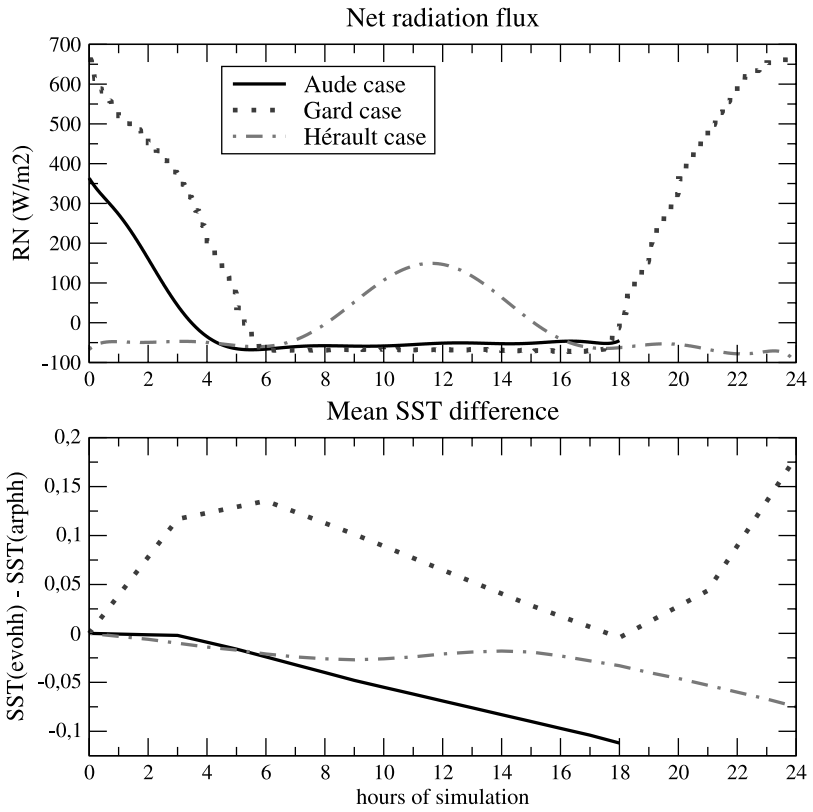

Figure 20. Temporal evolution of the difference between the evohh SST and the ARPEGE SST (°C) and of the net radiation (W m^{-2}) averaged over the 2.4-km sea grid for the three cases (solid curves for the Aude case, dotted curves for the Gard case and dashed-dotted curves for the Hérault case).

or decreasing the SST has almost no effect on the rainwater and snow contents, except between 0700 and 1300 UT during the first phase of the event when convection is more intense in stap3. Regarding the graupel content, lower (larger) contents are found when SST is decreased (increased) as for the two MCS cases. However graupel contents are not reduced (increased) significantly with time as in the previous cases. Moreover, after 1800 UT during the second phase of the event when the frontal dynamics dominates, stam3 and arp00 graupel contents are of the same order.

[48] Results of these sensitivity tests to the SST highlight that heavy precipitating systems do not respond identically to a prescribed SST perturbation. Indeed, for the two MCS cases, the SST impacts on the intensity and the localization of the convective activity. The warmer the SST, the more intense and less stationary the convection is. When the SST is too cold, the convection can be suppressed and replaced by stratiform precipitation or shallow orographic precipitation. For the second type of heavy precipitation events studied here (i.e., quasi-stationary frontal systems) the response to a SST change is more complex and includes interaction between deep convection and frontal dynamics. A weaker sensitivity to the SST is found when the frontal dynamics dominates.

4.4. Prognostic SST

[49] As mentioned in section 3.3.2, the evohh experiments start from the same SST fields as arphh, except that the SST is allowed to evolve with the model integration according to equation (1). Remember that the oceanic mixed layer temperature evolves because of the surface net heat flux. The aim of using a prognostic SST was to have a first idea of the impact of the low-level jet and of the strong convection on the oceanic mixed layer and to identify the feedbacks induced by an oceanic state change on the convective systems. This has been examined for the three cases. The evohh simulations are compared here to the arphh experiments, whatever the quality of the initial ARPEGE SST fields is.

[50] At the end of simulation evo12 for the Aude case, the SST has decreased by nearly 0.1°C on average both on the 9.5-km and 2.4-km domains (Figure 20). One part of this cooling of SST with time is due to the diurnal evolution of the net radiation R_N (Figure 20). Indeed a large part of the simulation takes place during the night. Cooling is also larger near the coast (Figure 21) because of strong and persistent latent heat air-sea fluxes under the easterly low-level jet that prevails over the Gulf of Lions during almost all the simulation. The SST decreases by 0.3°C in 18 hours, that constitutes a significant tendency value for a slow-evolving parameter as the SST. It is important noting that cooling beneath the convective precipitation produces the same tendency of SST cooling, but as it does not persist at the same location during all the simulation, no appreciable signature of the convective system is apparent in the SST field. Because of the cooling of SST, the latent and sensible heat surface fluxes are slightly weaker with time than those

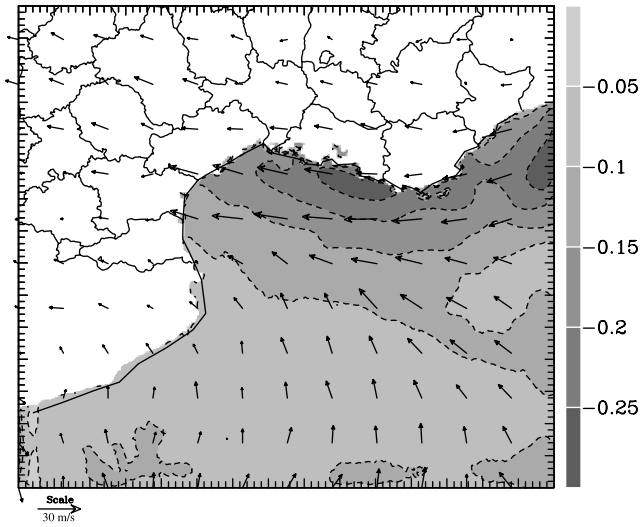

Figure 21. Difference between the SST field from evo12 and arp12 after 18 hours of simulation for the Aude case, superimposed to the 30-m AGL horizontal wind at 0600 UT, 13 November 1999, simulated by arp12.

of arp12 (not shown). This impact is however too weak to produce significant differences on the forecast of the MCS. The localization of the convective area is slightly modified, without however altering its intensity. Almost no difference is found for the low-level jet; The interpretation of these results has to take into account the short duration of the simulation (18 hours).

[51] In the evo00 simulation of the Hérault case, the decrease of SST with time is not as important as for the Aude case (only 0.08°C in 24 hours against more than 0.1°C in 18 hours, Figure 20). This is due to weaker surface fluxes, but also to a deeper oceanic mixed layer (35 m against 27 m), which implies more energy needed to decrease the SST by the same amount. Nevertheless, the decrease of SST in evo00 can locally reach 0.2°C. The evolution of the mean SST shows a diurnal cycle (Figure 20). During the day (between 1000 and 1700 UT), the net radiation (R_N) that is directly related to downward global solar flux, compensate the heat loss induced by the latent and sensible heat fluxes. Using an evolving SST modifies only slightly the simulation of the convection and of the low-level winds (Table 4).

[52] For the Gard case, because of weaker low-level winds over sea than in the other cases and no convection over sea, the SST evolution is principally governed by the net radiation, with a SST evolution following a diurnal cycle. The simulated SST tendencies are however more important than for the two other cases because of a thinner oceanic mixed layer; The SST is indeed increased by 0.18°C on average over the 2.4-km domain after 24 hours of simulation (Figure 20). Only small differences exist however between arp12 and evo12 in terms of localization of the convective cells or of their intensity (not shown).

[53] The evohh simulations do not perform significantly distinct atmospheric responses than the control runs. This is explained by small differences on average between the evolving SST at the end of the integration and the initial field from the ARPEGE SST analysis. Moreover, dense observations of SST miss to validate the evolving SST at local scale.

[54] Results with an evolving SST show that the SST tendencies obtained in 18–24 hours of simulation may be relevant for such a slow-evolving parameter, in particular underneath the low-level jet associated with the torrential rainfall events. However, its impact on very short range forecast of torrential events is limited.

5. Summary and Conclusions

[55] On the basis of numerical experiments of three representative cases of Mediterranean torrential rainfall events, we examined how the SST influences very short range (up to 18–24 hours) high-resolution (2–3 km) forecasts of heavy precipitating events. Results highlight that a warmer SST increases surface heat fluxes at the ocean-atmosphere interface, which in turn moisten and destabilize the low-level layers of the atmosphere up to 2000–3000 m. It results in an increase of the intensity of the convection and of the surface precipitation totals. On the other hand, a colder the SST weakens the sea surface heat fluxes. The low-level layers are less humid and less unstable. It reduces significantly the available energy for the convective system which therefore weakens and may even disappear after a few hours of simulation; Stratiform precipitation in that case dominates leading to a decrease of local rainfall totals. Some dynamical effects were also highlighted, but with different responses depending on cases. For the two MCS cases (Aude and Gard cases), the low-level jets are intensified (weakened) and the convective systems move more (less) rapidly if the SST is abnormally warm (cold). Nevertheless, for the Hérault case, the frontal perturbation progresses more rapidly when the SST is colder. The embedded convection, more intense when SST is increased, acts to slow down the westward advance of the front. This result is worth to be pointed out since the same kind of SST modifications can induce different atmospheric dynamical responses according to the meteorological type of the case studied.

[56] Using a higher-resolution SST field produces smaller-scale patterns in the surface heat fluxes fields, but has minor impacts on the convection or on low-level jets. Impacts of local anomalies of SST are smoothed by the spatial integration effect along the path of the low-level jet. This constitutes an important income for the next-generation high-resolution operational models; the use of high-resolution SST products seem not to be of primary importance for high-resolution quantitative precipitation forecasts of heavy

Table 4. Bias and RMS Errors From the Reference Experiment for the Simulation evo00 for the Hérault Case Computed Over the 2.4-km Domain

Simulation evo00	After 12 Hours	After 18 Hours	After 24 Hours
Accumulated precipitation, mm			
Bias	−0.051	−0.026	0.044
RMS	3.7	7.2	9.2
Latent heat flux over sea, W m^{-2}			
Bias	−1.0	0.6	−1.1
RMS	9.1	21.1	10.1

rainfall events. SST products at coarser resolution without significant mean bias error over the western Mediterranean basin (typically less than 0.5°C) appear to be sufficient for the heavy precipitating systems forecast by the next operational high-resolution short-range NWP systems. The relationship between the scale of the forecast process and the required scale of the resolved SST structures is only outlined here, and calls for a more thorough investigation in the future.

[57] Concerning the amplitudes of the increase/decrease applied to SST fields in our study, we can firstly state that errors in SST analyses are between 1 and 2°C. Tests with SST changes of 1.5°C show that these errors if they occur on a large enough scale may have a noticeable impact on high-resolution very short range forecasts of precipitating systems in terms of localization and intensity. If these analysis errors are limited in space, results of the noahh experiments show that they would almost not affect the high-resolution forecast of the precipitating systems. Our sensitivity tests must also be examined from the point of view of the climate warming. Climatic models forecast an increase ranging between 2.5 and 3.5°C of the Mediterranean SST by the end of the century, according to the selected climatic scenario [*Salas-Mélia et al.*, 2005; *Somot et al.*, 2006]. The SST perturbations of ±3°C performed in our study are therefore of the same amplitude than the SST increase forecasted by climate models and may provide a first indication of the possible impact of the climate warming on the western Mediterranean torrential rain events, through the assumption that the dynamics of the atmosphere remains the same. However, it is interesting to note that the absolute value of SST is not a discriminating factor for the MCS development. Indeed, the simulation of the Gard case in which the ARPEGE SST is decreased by 3°C (stam3) gives a mean SST much warmer than the mean of the Aude ARPEGE SST (arp12); however, for the stam3 simulation on the Gard case, the convection weakens whereas it is organized in a well developed convective system in the arp12 simulation on the Aude case. Not only the mean SST value makes different the Gard and the Aude events. For the Gard case, the conditional convective instability and consequently the thermal forcing and the air-sea temperature difference is an important ingredient for the MCS development. However, for the Aude case, dynamical forcing, e.g., a deep upper level trough associated in surface with a particularly strong easterly low-level jet seems to compensate the weaker convective instability.

[58] A simple coupling between the oceanic mixed layer and the atmosphere through a prognostic equation of the SST depending on the net surface fluxes and a prescribed depth of the oceanic mixed layer has been also developed and tested in the MESO-NH model in the framework of this study. It has small impacts on the convection and the low-level jets forecasts. However, it is expected that such coupling can provide improved background SST to the SST data assimilation, especially under disturbed atmospheric conditions. The experiments performed here are a first step toward a more complex coupling which will be able to take into account the turbulent exchanges inside the oceanic mixed layer and a greater number of interactions between the atmosphere and the ocean.

[59] The dependency of the results to the formulation of the heat surface fluxes parameterization is also currently examined, by testing various sea surface fluxes parameterizations. Results for the same cases as those discussed here will be described in a future paper.

Appendix A: Sea Surface Fluxes Equations in the MESO-NH Model

[60] In the MESO-NH model, the net radiation R_N (in W m^{-2}) is defined as the sum of the absorbed fractions of the incoming solar radiation R_G and of the atmospheric infrared radiation R_A, reduced by the emitted infrared radiation:

$$R_N = R_G(1-\alpha_t) + \epsilon_t\left(R_A - \sigma_{SB}T_s^4\right) \tag{A1}$$

where α_t, ε_t and T_s are the albedo, the emittance and the temperature (in K) of the surface, respectively; σ_{SB} is Stefan-Boltzmann constant.

[61] The sea surface heat fluxes equations follows a bulk parameterization defined as:

$$H = \rho_a c_p C_H v_a (T_s - T_a) \tag{A2}$$

$$LE = \rho_a c_p C_H v_a (q_{sat}(T_s) - q_a) \tag{A3}$$

for the sensible H and the latent LE heat fluxes (W m^{-2}) positive toward the atmosphere; where c_p is the specific heat; ρ_a, v_a, T_a and q_a are the air density, the wind speed, the temperature, and the atmospheric specific humidity at the lowest atmospheric level, respectively; $q_{sat}(T_s)$ is the saturated specific humidity at the temperature T_s. C_H is the heat transfer coefficient depending on the thermal stability of the atmosphere.

[62] **Acknowledgments.** Our gratitude goes to the Centre de Météo Spatiale of Lannion which provided us satellite data and to Silvana Ramos Buarque who helped us to produce the 2.5-km resolution satellite SST fields. The authors are grateful to the three anonymous reviewers, who provided us useful recommendations.

References

AVELMOR (2002), Développement d'une analyse de température de surface de la mer échelle fine au Centre de Météo Spatiale de Météo-France, technical report, Plouzané, France.

Bahurel, P., E. Dombrowsky, J. M. Lellouche, and the Mercator Project Team (2004), Mercator ocean monitoring and forecasting system, near-realtime assimilation of satellite and in-situ data in different operational ocean models, paper presented at 36th Colloquium on Ocean Dynamics, Geohydrodyn. and Environ. Res. Group, Univ. of Liége, Liège, Belgium.

Bao, J.-W., J. M. Wilczak, J.-K. Choi, and L. H. Kantha (2000), Numerical simulations of air-sea interaction under high wind conditions using a coupled model: A study of hurricane development, *Mon. Weather Rev.*, *128*, 2190–2210.

Bechtold, P., and E. Bazile (2001), The 12–13 November 1999 flash flood in southern France, *Atmos. Res.*, *56*, 171–189.

Bechtold, P., E. Bazile, F. Guichard, P. Mascart, and E. Richard (2001), A mass flux convection scheme for regional and global models, *Q. J. R. Meteorol. Soc.*, *127*, 869–886.

Bender, M. A., and I. Ginis (2000), Real-case simulations of hurricane-ocean interaction using a high-resolution coupled model: Effects on hurricane intensity, *Mon. Weather Rev.*, *128*, 917–946.

Caniaux, G., J.-L. Redelsperger, and J.-P. Lafore (1994), Parametrization of orography-induced turbulence in a meso-beta scale model, *Mon. Weather Rev.*, *117*, 1870–1888.

Delrieu, G., et al. (2005), The catastrophic flash-flood event of 8–9 September 2002 in the Gard region, France: Mediterranean Hydro-meteorological Observatory, *J. Hydrometeorol.*, *6*, 34–51.

Doswell, C. A., III, C. Ramis, R. Romero, and S. Alonso (1998), A diagnostic study of three heavy precipitation episodes in the western Mediterranean region, *Weather Forecasting*, *13*, 102–124.

Ducrocq, V., D. Ricard, J. P. Lafore, and F. Orain (2000), Initialisation of a fine scale model for convective system prediction: A case study, *Q. J. R. Meteorol. Soc.*, *126*, 3041–3066.

Ducrocq, V., D. Ricard, J. P. Lafore, and F. Orain (2002), Storm-scale numerical rainfall prediction for five precipitating events over France: On the importance of the initial humidity field, *Weather Forecasting*, *17*, 1236–1256.

Ducrocq, V., G. Aullo, and P. Santurette (2003a), Les précipitations intenses et les inondations des 12 et 13 novembre 1999 sur le sud de la France, *Meteorologie*, *42*, 18–27.

Ducrocq, V., K. Chancibault, F. Habets, and S. Anquetin (2003b), Mesoscale modelling of a flooding storm. Application to the extreme flood of Gard, Mediterranean storms, paper presented at 5th EGS Plinius Conference, Eur. Geophys. Soc., Ajaccio, France, 1–3 Oct.

Ducrocq, V., C. Lebeaupin, T. Touvenin, H. Giordani, K. Chancibault, S. Anquetin, and G.-M. Saulnier (2004), L'événement des 8 et 9 Septembre 2002: Situation météorologique et simulation á méso-échelle, *Houille Blanche*, *6*, 86–92.

Gal-Chen, T., and R. Sommerville (1975), On the use of a coordinate transformation for the solution of the Navier-Stokes equations, *J. Comput. Phys.*, *17*, 209–228.

Gao, X., S. Sorooshian, J. Li, and J. Xu (2003), SST data improve modelling of North American monsoon rainfall, *Eos Trans. AGU*, *84*(43), 457–462.

Gaspar, P. (1988), Modelling of seasonal cycle of the upper ocean, *J. Phys. Oceanogr.*, *18*(2), 161–180.

Giordani, H., and G. Caniaux (2001), Sensivity of cyclogenesis to sea surface temperature in the northwestern Atlantic, *Mon. Weather Rev.*, *129*, 1273–1295.

Giordani, H., and S. Planton (2000), Modelling and analysis of ageostrophic circulation over the Azores oceanic front during the SEMAPHORE experiment, *Mon. Weather Rev.*, *128*, 2270–2287.

Giordani, H., S. Planton, B. Benech, and B.-H. Kwon (1998), Atmospheric boundary layer response to sea surface temperatures during the SEMAPHORE experiment, *J. Geophys. Res.*, *103*(C11), 25,047–25,060.

Homar, V., R. Romero, C. Ramis, and S. Alonso (2002), Numerical study of the October 2000 torrential precipitation event over eastern Spain: Analysis of the synoptic-scale stationarity, *Ann. Geophys.*, *20*, 2047–2066.

Homar, V., R. Romero, D. J. Stensrud, C. Ramis, and S. Alonso (2003), Numerical diagnosis of a small, quasi-tropical cyclone over the western Mediterranean: Dynamical vs. boundary factors, *Q. J. R. Meteorol. Soc.*, *129*, 1469–1490.

Lafore, J.-P., et al. (1998), The MESO-NH atmospheric simulation system. Part I: Adiabatic formulation and control simulations, *Ann. Geophys.*, *16*, 90–109.

Levitus, S. (1982), Climatological atlas of the World Ocean, *Prof. Pap. 13*, 173 pp. and 17 microfiche, NOAA/ERL Geophys. Fluid Dyn. Lab., Princeton, N. J.

McClain, E. P., W. G. Pichel, and C. C. Walton (1985), Comparative performance of AVHRR based multichannel sea surface temperature, *J. Geophys. Res.*, *90*, 11,587–11,601.

Millan, M. M., M. J. Estrela, and V. Caselles (1995), Torrential precipitations on the Spanish east coast: The role of the mediterranean sea surface temperature, *Atmos. Res.*, *36*, 1–16.

Pastor, F., M. J. Estrela, P. Penarrocha, and M. M. Millan (2001), Torrential rains on the spanish Mediterranean coast: Modelling the effect of the sea surface temperature, *J. Appl. Meteorol.*, *40*, 1180–1195.

Pinty, J. P., and P. Jabouille (1998), A mixed-phased cloud parametrizations for use in a mesoscale non-hydrostatic model: Simulation of a squall line and orographic precipitation, paper presented at Conference on Cloud Physics, Am. Meteorol. Soc., Everett, Wash.

Ramos Buarque, S., and G. Caniaux (2003), High-resolution gridded air-sea surface fluxes over the Mediterranean basin by a synthesis approach, internal technical report, CNRM/GAME-GMGEC, Toulouse, France.

Romero, R., C. Ramis, and S. Alonso (1997), Numerical simulation of an extreme rainfall event in Catalonia: Role of orography and evaporation from the sea, *Q. J. R. Meteorol. Soc.*, *123*, 537–559.

Rowell, D. P. (2003), The impact of Mediterranean SSTs on the Sahelian rainfall season, *J. Clim.*, *16*(5), 849–862.

Salas-Mélia, D., F. Chauvin, M.|Déqué, H. Diouville, J. F. Guemery, P. Marquet, S. Planton, J. F. Royer, and S. Tyteca (2005), XXth century warming simulated by ARPEGE-Climat-OPA coupled system, *Note 103*, Cent. GAME/GMGEC, Toulouse, France.

Scofield, R. A. (1985), Satellite convective categories associated with heavy precipitation, paper presented at Sixth Conference on Hydrometeorology, Am. Meteorol. Soc., Indianapolis, Indiana.

Shade, L. R., and K. A. Emanuel (1999), The ocean's effect on the intensity of tropical cyclones: Results from a simple coupled atmosphere-ocean model, *J. Atmos. Sci.*, *56*, 642–651.

Somot, S., F. Sevault, and M. Déqué (2006), Transient climate change scenario simulation of the Mediterranean Sea for the 21st century using a high resolution ocean circulation model, *Clim. Dyn.*, in press.

Weill, A., et al. (2003), Toward better determination of turbulent air-sea fluxes from several experiments, *J. Clim.*, *16*, 600–618.

V. Ducrocq, H. Giordani, and C. Lebeaupin, Centre National de Recherches Meteorologiques/Groupe d'étude de l'Atmosphre Metéorologique, 42 avenue G. Coriolis, F-31057 Toulouse cedex, France. (cindy.lebeaupin@cnrm.meteo.fr)